

*Annual Review of Biomedical Engineering*  
**Conformable Piezoelectric  
 Devices and Systems for  
 Advanced Wearable and  
 Implantable Biomedical  
 Applications**

Jin-Hoon Kim,\* Hyeokjun Yoon,\* Shrihari Viswanath,\*  
 and Canan Dagdeviren

Media Lab, Massachusetts Institute of Technology, Cambridge, Massachusetts, USA;  
 email: canand@media.mit.edu

ANNUAL  
REVIEWS **CONNECT**

[www.annualreviews.org](http://www.annualreviews.org)

- Download figures
- Navigate cited references
- Keyword search
- Explore related articles
- Share via email or social media

Annu. Rev. Biomed. Eng. 2025. 27:255–82

The *Annual Review of Biomedical Engineering* is  
 online at [bioeng.annualreviews.org](http://bioeng.annualreviews.org)

<https://doi.org/10.1146/annurev-bioeng-020524-121438>

Copyright © 2025 by the author(s). This work is  
 licensed under a Creative Commons Attribution 4.0  
 International License, which permits unrestricted  
 use, distribution, and reproduction in any medium,  
 provided the original author and source are credited.  
 See credit lines of images or other third-party  
 material in this article for license information.

\*These authors contributed equally to this article



### Keywords

conformable electronics, piezoelectric materials, electromechanical  
 transducers, biomedical devices

### Abstract

With increasing demands for continuous health monitoring remotely, wearable and implantable devices have attracted considerable interest. To fulfill such demands, novel materials and device structures have been investigated, since commercial biomedical devices are not compatible with flexible and conformable form factors needed for soft tissue monitoring and intervention. Among various materials, piezoelectric materials have been widely adopted for multiple applications including sensing, energy harvesting, neurostimulation, drug delivery, and ultrasound imaging owing to their unique electromechanical conversion properties. In this review, we provide a comprehensive overview of piezoelectric-based wearable and implantable biomedical devices. We first provide the basic principles of piezoelectric devices and device design strategies for wearable and implantable form factors. Then, we discuss various state-of-the-art applications of wearable and implantable piezoelectric devices and their design strategies. Finally, we demonstrate several challenges and outlooks for designing piezoelectric-based conformable biomedical devices.

## Contents

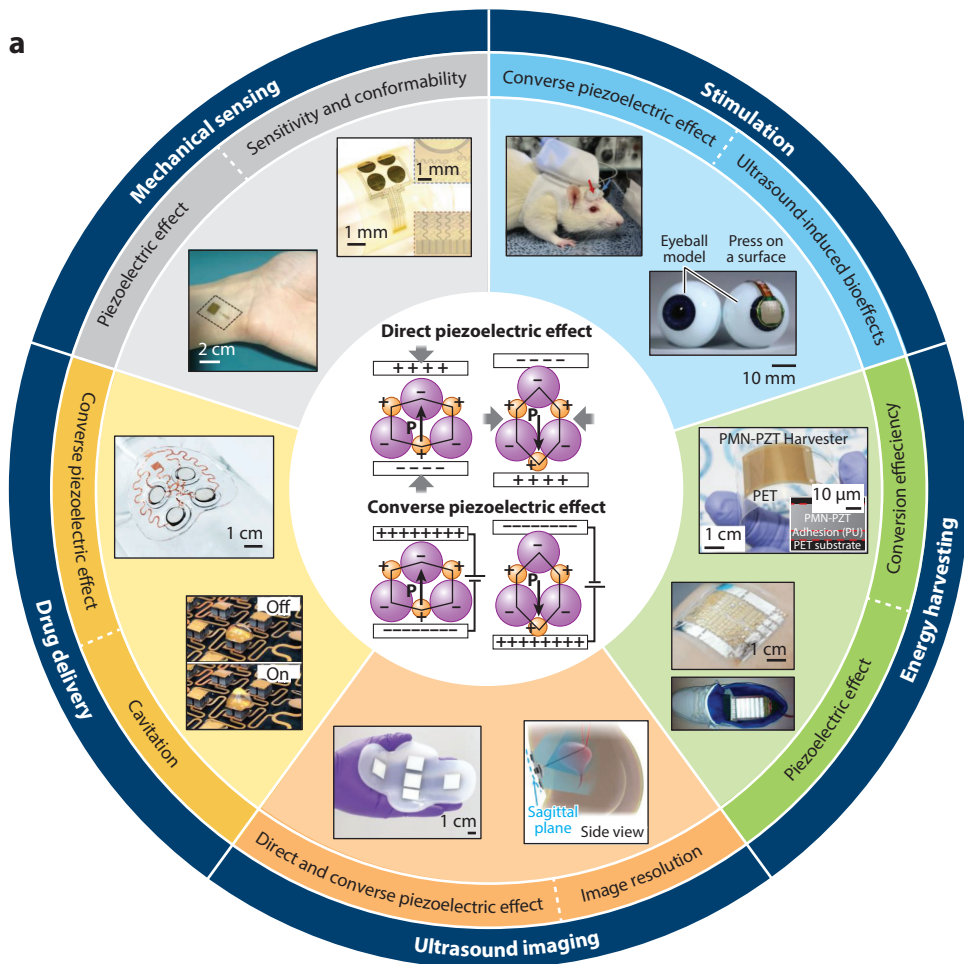
|   |     |
|---|-----|
| 1. INTRODUCTION .....   | 256 |
| 2. PRINCIPLES AND STATE-OF-THE-ART EXAMPLES OF<br>ULTRASOUND TECHNOLOGIES IN BIOMEDICAL APPLICATIONS .... | 258 |
| 2.1. Energy Harvesting .....  | 258 |
| 2.2. Mechanical Sensing .....   | 262 |
| 2.3. Neurostimulation .....   | 264 |
| 2.4. Drug Delivery .....  | 267 |
| 2.5. Ultrasound Imaging .....   | 270 |
| 3. CONCLUSION AND OUTLOOKS .....  | 274 |

## 1. INTRODUCTION

As civilization advances rapidly, technology plays a pivotal role in improving healthcare accessibility across the globe and furnishing enhanced medical treatments to patients equitably (1). Thanks to the development of novel materials, devices, and analysis techniques, medical institutes have numerous healthcare capabilities, significantly improving survival rates and quality of life (2). In today's evolving health landscape, there is an additional demand for personalized medicine, at-home therapy, telehealth, and early intervention (3, 4). However, conventional biomedical instruments and devices are often rigid and bulky, making them unsuitable and uncomfortable for continuous usage (5, 6). Furthermore, given the high prices of these devices, they are not easily accessible to the majority of people around the world (7). In addressing such needs, advanced medical technologies including wearable and implantable devices emerge as crucial tools, alleviating the burden on the healthcare systems, reducing medical costs, and improving the quality of care (6). In particular, conformable form factors for safe and seamless integration of wearable and implantable devices with soft tissue have been vigorously investigated (4, 8).

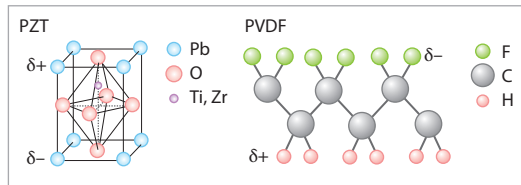
Among various materials implemented for conformable wearable and implantable biomedical devices, piezoelectric materials have drawn large interest owing to their unique physical properties, as shown in **Figure 1** (9, 10). Piezoelectric materials can generate electrical signals in response to mechanical stress or strain (**Figure 1a**), making them suitable candidates for contact-based wearables that are exceptionally sensitive to physiological movements and forces (10). Moreover, piezoelectric energy harvesters, which also utilize direct piezoelectric effects, have also shown great potential to address power limitations in wearable and implantable devices (11, 12). By converting kinetic energy into electrical energy, they can provide a crucial power source for these systems (13).

In contrast to the direct piezoelectric effect, the converse piezoelectric effect enables the generation of mechanical (ultrasound) waves, which can propagate through the body to reach deep tissues, enabling comprehensive monitoring and therapeutic applications, as shown in **Figure 1a** (14, 15). Recently, research into ultrasound-induced bioeffects (16) has expanded the biomedical uses of piezoelectric materials to stimulation and drug delivery, thereby significantly broadening their applications to encompass both induced bioeffects and passive sensing capabilities (17, 18). Wide pools of piezoelectric materials offer significant advantages for both implantable and wearable healthcare technologies. Biocompatible inorganic piezo-materials provide robust and reliable performance without eliciting adverse biological responses (19). Meanwhile, biodegradable organic piezoelectric materials offer the additional benefit of breaking down safely within



**b**

**Piezoelectric materials**



**Piezoelectric coefficient (d)**

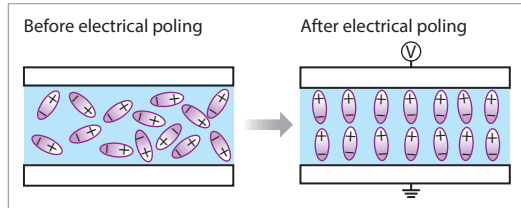
$$d = \frac{\text{Developed strain}}{\text{Applied electrical field}} = \frac{\text{Charge density}}{\text{Applied stress}}$$

$$d_{31} = k_{31} \sqrt{\epsilon_0 k_{33}^T \epsilon_{11}^E} \quad k^T = \text{Relative dielectric constant}$$

$$d_{33} = k_{33} \sqrt{\epsilon_0 k_{33}^T \epsilon_{33}^E} \quad \epsilon^E = \text{Elastic compliance}$$

$$\epsilon_0 = \text{Vacuum dielectric permittivity}$$

**Electrical poling**



**Electromechanical coupling coefficient (k)**

$$k = \sqrt{\frac{\text{Converted mechanical energy}}{\text{Applied electrical energy}}}$$

$$= \sqrt{\frac{\text{Converted electrical energy}}{\text{Applied mechanical energy}}}$$

$$k_{\text{eff}}^2 = 1 - \left(\frac{f_r}{f_a}\right)^2 \quad k_{\text{eff}} = \text{Effective coupling coefficient with an arbitrary shape}$$

(Caption appears on following page)

**Figure 1** (Figure appears on preceding page)

(a) Overview of piezoelectric-based wearable and implantable devices for biomedical applications. Direct and converse piezoelectric effects of piezoelectric materials enable electromechanical transducing for diverse applications including energy harvesting, mechanical sensing, stimulation, drug delivery, and ultrasound imaging. Mechanical sensing panels adapted from References 51 and 54 with permission from Springer Nature. Stimulation panels adapted from Reference 101 (CC BY 4.0) and from Reference 104 with permission from Springer Nature. Energy harvesting panels adapted from Reference 34 with permission from Wiley-VCH, from Reference 43 with permission from Springer Nature, and from Reference 46 (CC BY 4.0). Ultrasound imaging panels adapted from Reference 146 with permission from Springer Nature. Drug delivery panels adapted from Reference 17 with permission from Wiley-VCH and from Reference 105 with permission from American Chemical Society. (b) Several fundamental definitions of piezoelectricity including basic structures of piezoelectric materials (*top left*), piezoelectric coefficient  $d$  (*top right*), electrical poling (*bottom left*), and electromechanical coupling coefficient  $k$  (*bottom right*). Abbreviations: PET, poly(ethylene terephthalate); PMN, lead-magnesium-niobate lead-titanate; PU, polyurethane; PVDF, poly(vinylidene fluoride); PZT, lead zirconate titanate.

the body, making them ideal for temporary implants and reducing long-term complications and additional operations for device extraction (19).

Although there are several key advantages of piezoelectric materials for wearable and implantable devices, there are still several challenges to be overcome. In this review, we provide an intensive overview of the latest breakthroughs and advancements in conformable piezoelectric technologies for wearable and implantable biomedical applications. The term conformability indicates the ability to make a seamless contact with soft tissues even under dynamic motions. The key works that have resolved these limitations and have helped realize some of the current state-of-the-art research are covered in the upcoming sections. We address various applications of piezoelectric devices, including mechanical sensing, energy harvesting, drug delivery, neurostimulation, and ultrasound imaging. Finally, future outlooks for next-generation piezoelectric material-based conformable devices are detailed.

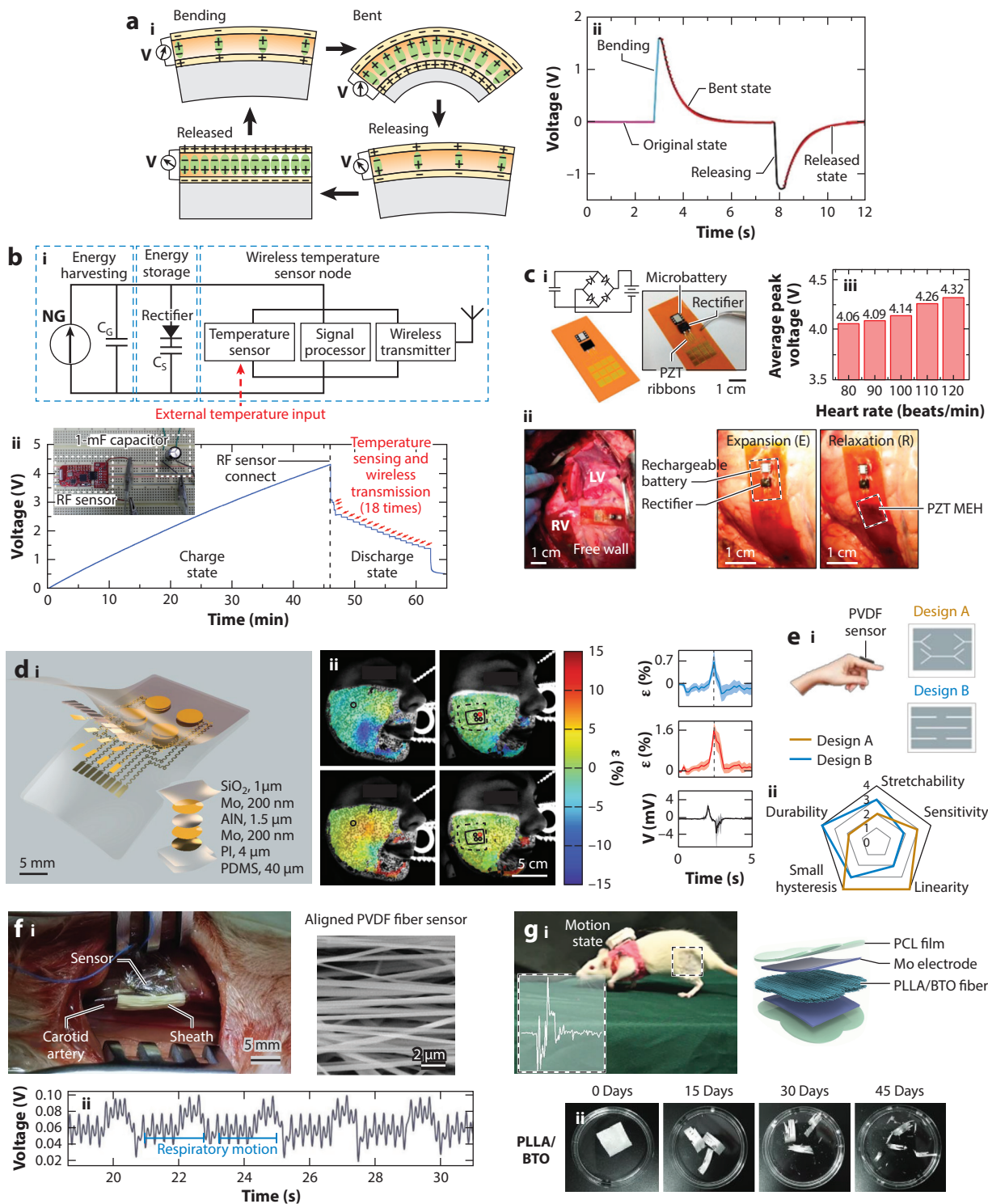
## 2. PRINCIPLES AND STATE-OF-THE-ART EXAMPLES OF ULTRASOUND TECHNOLOGIES IN BIOMEDICAL APPLICATIONS

In this section, we introduce some state-of-the-art wearable and implantable devices utilizing direct (energy harvesting and mechanical sensing) and converse (neurostimulation, drug delivery, and ultrasound imaging) piezoelectric effects. Brief working principles of each application are provided, and practical examples with novel approaches are discussed.

### 2.1. Energy Harvesting

In most wearable electronics, rechargeable batteries are utilized for the power sources, which have limited lifetimes and size constraints. Thus, repetitive charging is necessary, which is uncomfortable for the users. This issue is even more critical for implantable devices such as pacemakers, as battery replacement necessitates additional postimplantation surgery. Hence, harvesting energy from environments including solar power, body heat, fluid, and motion has become of great interest (20, 21), as such harvested energy can directly operate the devices or charge the batteries. Among these approaches, harvesting energy from body motion contains great potential since it can generate a high amount of kinetic energy for the power source of wearable devices (22, 23).

Among various materials, piezoelectric materials are potential candidates for harvesting such kinetic energy from body motion. Piezoelectric materials can generate an electrical field when they are mechanically pressed or flexed, as shown in **Figure 2a**. When two electrodes are formed at the top and bottom surfaces of the piezoelectric material, and external electrical loads (external resistance, capacitor, battery, etc.) are connected to these electrodes, the electrical current induced from piezoelectric materials by external mechanical deformations can flow through the external circuit, as shown in **Figure 2b**. The generated current can perform various tasks



(Caption appears on following page)

Energy harvesting and mechanical sensing. (a) Electromechanical transduction mechanism of piezoelectric materials. Deformation of the material (i) induces voltage generation when bending and releasing occur (ii). (b) Wireless temperature sensing circuit operated by PZT-based energy harvester (i). The generated energy is stored in a capacitor, which can be discharged for temperature sensor operation and RF communication (ii). (c) Implantable PZT-based energy harvester storing energy by changing induced AC signals into DC signals by a rectifier circuit (i). An implantable device attached on the heart (ii) can conduct energy harvesting, whose average peak voltage is dependent on the frequency of the heartbeat (iii). (d) Thin-film AlN-based wearable strain sensor array (i) for facial motion detection (ii). (e) Kirigami cutting method for fabricating a stretchable PVDF-based mechanical sensor (i), demonstrating different characteristics based on different device designs (ii). (f) Electrospun PVDF fiber-based implantable mechanical sensor (i) for blood pulse monitoring on carotid artery (ii). (g) BTO-doped PLLA fiber-based mechanical sensor for injury recovery monitoring on sciatic nerve (i), which shows biodegradability (ii). Abbreviations: AC, alternating current; BTO, BaTiO<sub>3</sub>; DC, direct current; LV, left ventricle; MEH, mechanical energy harvester; Mo, molybdenum; NG, nanogenerator; PCL, polycaprolactone; PDMS, polydimethylsiloxane; PLLA, poly-L-lactide; PVDF, poly(vinylidene fluoride); PZT, lead zirconate titanate; RF, radiofrequency; RV, right ventricle. Panel a, subpanel ii adapted from Reference 27 with permission from Springer Nature. Panel b adapted from Reference 25 with permission from Wiley-VCH. Panel c adapted from Reference 11 with permission from National Academy of Science. Panel d adapted from Reference 54 with permission from Springer Nature. Panel e adapted from Reference 55 with permission from Springer Nature. Panel f adapted from Reference 77 with permission from Wiley-VCH. Panel g adapted from Reference 79 with permission from Wiley-VCH.

including charging batteries and capacitors and allowing the operation of self-powered sensors (11, 24, 25).

In this section, the working principles of piezoelectric materials, design strategies, and their applications for energy harvesting are discussed. For a wearable piezoelectric energy harvester, the main deformation mode is the bending mode based on a thin and flexible form factor (11, 25, 26). While the piezoelectric energy harvester is undergoing convex bending, as shown in **Figure 2a**, positive and negative piezoelectric potentials are generated on the top and bottom of the piezoelectric layer, respectively, due to the mechanical stress induced by the mechanical bending. When the top and bottom electrodes are connected to the external circuit, electrons will flow into and out of the top and bottom electrode, respectively, to balance the electric field induced within the piezoelectric layer. Such electron flow generates electrical current, and the amount of the current will increase and reach the maximum value when the bending radius is the highest, as shown in **Figure 2a**. While the piezoelectric energy harvester maintains a bent state, the electrical flow will relax to zero, as shown in **Figure 2a** (27). When the piezoelectric energy harvester starts to relax back to the flat state, the electric field induced by the piezoelectric effect will diminish, accompanying the opposite electrical current, as shown in **Figure 2a**. This opposite current flow will reach maximum magnitude when the device reaches the flat state. When the piezoelectric energy harvester undergoes concave bending, the electric field will be applied with the opposite polarity.

The exact dynamics of voltage and current under the mechanical deformation of the piezoelectric energy harvester can be calculated using plate bending and piezoelectric theories (11, 28). As shown in **Figure 2a**, electrical current is generated only during the dynamic deformation of the piezoelectric energy harvester. Hence, the frequency of the deformation is critical in the energy harvesting performance of the piezoelectric energy harvester. Since the generated current shows alternating current (AC) characteristics, a rectifier circuit is generally required when a direct current (DC) source is needed (charging the battery, etc.), as shown in **Figure 2b,c**.

Several material and structural design approaches can be considered to develop high-performance wearable piezoelectric energy harvesters. When selecting the piezoelectric material, materials with a high piezoelectric coefficient  $d$  (described in **Figure 1b**) are preferred due to their high energy conversion efficiency (11, 29–31). Piezoelectric ceramics exhibit a cubic-like perovskite structure, which can be polarized from an external electric field to reorganize the polarization vectors within the structure, called a poling process, as described in **Figure 1b** (25). Such a poling process endows the macroscale piezoelectric effect by preventing the canceling

of the induced electrical field, allowing the highly efficient direct piezoelectric effect for energy harvesting and mechanical sensing. Among various materials, inorganic ceramics such as lead zirconate titanate [Pb(Zr<sub>1-x</sub>Ti<sub>x</sub>)O<sub>3</sub>] (PZT), Pb(Mg<sub>1/3</sub>Nb<sub>2/3</sub>)O<sub>3-x</sub>PbTiO<sub>3</sub> (PMN-PT), BaTiO<sub>3</sub> (BTO), K<sub>1/2</sub>Na<sub>1/2</sub>NbO<sub>3</sub> (KNN), and AlN have been explored for wearable and implantable applications (11, 25, 31–34). Although such inorganic piezoelectric materials have high energy conversion efficiency, their inherent brittleness is a major challenge in applying them to wearable energy harvesters.

Hence, various strategies have been investigated to cope with this limitation. The first approach is to make the device thinner. According to the mechanics of materials, the bending stiffness of the films is proportional to Young's modulus and the cube of the thickness of the devices (35). As the thin film structure allows high bending curvature while maintaining the strain below the fracture threshold, the strategy can endow higher conformability and flexibility to the piezoelectric ceramics on soft tissue interfaces. For instance, when a PZT-based thin film piezoelectric energy harvester with a total thickness of 77.2 μm [polyimide (PI) (1.2 μm)/Au (200 nm)/Cr (20 nm)/PZT (500 nm)/Pt (300 nm)/Ti (20 nm)/PI (75 μm)] was fabricated, the maximum bending strain applied to the PZT layer under 25 mm of bending radius was only 0.1%, lower than the fracture strain of PZT (11).

Another approach is using inorganic nanomaterials including nanoparticles (NPs) and nanowires (NWs). NPs can easily be embedded into flexible and soft polymer matrices, providing high mechanical flexibility and even stretchability. Various inorganic NPs based on BTO, KNN, and PZT have been incorporated into soft organic materials and showed good energy harvesting performances (36–38). Vertically aligned inorganic piezoelectric NWs based on BTO, GaN, or ZnO can be utilized as flexible energy harvesters (39, 40). Owing to their geometry being insensitive to in-plane bending, vertically aligned inorganic NW-based harvesters could possess high power density. Waseem et al. (41) reported flexible piezoelectric energy harvesters based on Mg-doped GaN (GaN:Mg)/ZnO core-shell NWs. They achieved a power density of 170 μW/cm<sup>2</sup> at a load resistance of 2.5 MΩ (41).

Organic piezoelectric materials are also promising candidates for wearable piezoelectric energy harvesters due to their excellent mechanical flexibility and conformability (29, 42, 43). To enhance the harvesting performance of organic piezoelectric materials, various materials have been investigated. Among them, fluoropolymer-based poly(vinylidene fluoride) (PVDF)-based materials showed great piezoelectric performance owing to the fluorine atom in the polymer chain, as shown in **Figure 1b** (29). The various fabrication method options are another advantage of organic piezoelectric materials. Electrospinning has been widely adopted, since simultaneous mechanical stretching and electrical poling are applied to the spun fiber during fabrication, which enhances the piezoelectric performance significantly (44). Moreover, inorganic NPs can be incorporated into PVDF fibers during the electrospinning process to further enhance the piezoelectric performance (36–38). Qin et al. (45) reported a Bi<sub>3.15</sub>Nd<sub>0.85</sub>Ti<sub>3</sub>O<sub>12</sub> microsphere-embedded PVDF-hexafluoropropylene (PVDF-HFP)-based flexible piezoelectric energy harvester. They recorded a power density of 938 μW/cm<sup>2</sup> at a load resistance of 10 MΩ (45).

Developed piezoelectric energy harvesters are usually applied to the lower limbs in locations such as the hip joint, knee, ankle, and foot due to the high kinetic energy and continuous periodic motions of these areas during walking and running (22, 46). It has been shown that flexible and wearable piezoelectric energy harvesters can charge batteries in the circuit to perform various activities. Hwang et al. (25) developed PZT-based flexible energy harvesters with interdigitated electrode geometry. By transfer-printing high-quality PZT layers onto a flexible substrate using an inorganic-based laser lift-off method, they obtained a piezoelectric energy harvester with an

output power of 200  $\mu\text{W}$ , which is enough for charging a 1-mF capacitor. By using this device, they could directly charge a supercapacitor, operate a temperature sensor, and transmit the data through radiofrequency (RF) communication for 18 repetitive cycles without recharging, as shown in **Figure 2b** (25).

As mentioned above, power management of implantable devices is extremely crucial. Various internal organs such as the heart, lung, diaphragm, intestines, and stomach are constantly in motion, which makes them good sources for mechanical energy harvesting (11, 33). Hence, integrating an energy harvester with implantable devices could be a good method to extend the battery life of the devices. Dagdeviren et al. (11) reported a PZT-based flexible piezoelectric device for harvesting mechanical energy from the heart, as shown in **Figure 2c**. They integrated the device with a rectifier and microbattery, demonstrating that PZT-based energy harvesters could charge the battery while attached to the heart, lung, and diaphragm on a pig model in vivo (11). They also showed that by optimizing the device orientation and stacking, the device could generate enough electrical power for operating a commercial pacemaker (11). Recent progress in the development of piezoelectric energy harvesting devices has shown that they have strong potential as power sources for wearable and implantable electronic devices, but their low power conversion efficiency should be improved to charge electronics with high power consumption such as smartwatches. The conversion efficiency of piezoelectric energy harvesters can be enhanced by utilizing various approaches, including: (a) improving the piezoelectric properties of materials (29), (b) adopting novel device structures such as nanotextures (47), (c) engineering the harvester geometry to match the resonance frequency with the dominant motion's vibration frequency (47), and (d) optimizing the electrical circuit for impedance matching and adjusting the electrical load to extract maximum electrical power (48).

## 2.2. Mechanical Sensing

The electromechanical transducing effect from the piezoelectric materials introduced above can also decode mechanical deformation. Due to the simple mechanism and high sensitivity of piezoelectric material-based devices, mechanical sensing is one of the most basic applications, and it has shown high effectiveness for diverse biomedical utilizations. By utilizing the direct piezoelectric effect, which transduces mechanical deformation into an electrical signal, diverse modalities including pressure (49–53), strain (54–56), modulus (57, 58), acoustics (59–61), and acceleration (62) can be effectively decoded. In particular, recently studied mechanically compliant piezoelectric mechanical sensors have been successfully integrated with soft tissue, so that they enable diverse wearable biomechanics decoding (19, 63–65). Here, we demonstrate wearable and implantable mechanical sensors fabricated with various piezoelectric materials and diverse form factors.

Similar to the piezoelectric energy harvesters discussed in Section 2.1, the most popular and widely used materials for wearable mechanical sensing are piezoelectric ceramics. Piezoelectric ceramics generally show high  $d$ , which reflects the electromechanical transducing efficiency (66). To cope with the inherent brittleness of inorganic piezoelectric material, similar ultrathin geometry has been adopted, as mentioned in the previous section. For instance, Dagdeviren et al. (51) demonstrated a PZT-based cutaneous pressure monitoring device that implemented 400-nm-thick PZT films. Since decoded cutaneous pressure can reflect the arterial pulse information, the device can be utilized for daily health monitoring. Moreover, blood pressure can be efficiently estimated by applying multiple piezoelectric pressure sensors. In addition, by incorporating the converse piezoelectric effect, the viscoelasticity of the skin can be also measured through PZT-based conformable actuator–sensor pairs whose active layer thickness is 500 nm (57). When the actuator induces mechanical motions generated by the converse piezoelectric effect through

integrated tissues, the sensor can decode the motion through voltage response via the direct piezoelectric effect. This mechanism enables measurement of the modulus of skin, which can be used for pathology mapping of lesions from skin cancer on various human tissues including face and leg tissues. Moreover, it is also applicable to measure the modulus of various organs including the lungs, ventricles, and apex of the heart (57).

In addition to PZT, other ceramic materials can be also effectively adopted for conformable mechanical sensing applications. For example, a conformable piezoelectric sensor array utilizing AlN (thickness: 1.5  $\mu\text{m}$ ) as the active piezoelectric material enabled facial motion detection for both healthy subjects and patients with neuromuscular diseases (e.g., amyotrophic lateral sclerosis), as described in **Figure 2d** (54). By integrating machine learning signal analysis methods including k-nearest neighbor and dynamic time warping, the conformable device successfully classified various facial motions, and this application is expected to be utilized for language classification and human–machine interfaces. Furthermore, to enhance the piezoelectricity, rare elements have been adopted as a doping material for piezoelectric ceramics. For example, Sm-doped PMN-PT (thickness: 850 nm) was harnessed for motion detection of various body parts including the wrist, fingers, and foot (67).

Despite the high piezoelectric performance of inorganic materials, their brittleness limits their application to a low range of deformation. In this regard, organic piezoelectric materials have been widely investigated for mechanical sensors owing to their good flexibility and conformability (66). For example, Chiu et al. (68) harnessed commercial PVDF film (thickness: 25  $\mu\text{m}$ ) for heartbeat and respiration monitoring by decoding the output voltage variance from the film. In addition, PVDF fiber-based mechanical sensors, which have the advantage of higher flexibility and easy integration with commercial clothes, have also been investigated (64). Persano et al. (62) utilized electrospinning technology to manufacture poly(vinylidene fluoride-cotrifluoroethylene) [P(VDF-TrFe)] fiber-based sensors for pressure sensors and accelerometers. Doping with inorganic piezoelectric materials has been shown to be a highly effective method for enhancing the electromechanical coupling coefficient  $k$  (described in **Figure 1b**) of polymer-based piezoelectric materials, as mentioned in Section 2.1. For example, electrospun BTO-doped PVDF fiber exhibited high sensitivity and long stability while maintaining the flexible characteristics of the polymer materials (69). Moreover, piezoelectric yarns fabricated by twisting electrospun BTO-doped P(VDF-TrFe) demonstrated robust strength with enhanced piezoelectric performance when utilized for wearable mechanical sensors attached to socks for motion classification (70).

Another notable strategy to enhance the operation range of piezoelectric material-based mechanical sensors is integrating a kirigami structure (71). A kirigami structure enables a high degree of stretchability for both piezoelectric ceramics and piezoelectric polymers for efficient strain sensing at a high degree of strain. For example, Hong et al. (72) utilized a PZT composite-coated kirigami-structured textile for joint motion sensing for preventing musculoskeletal disorders including neck pain and shoulder fatigue by continuously monitoring joint bending direction, bending radius, and types of motions of the upper body terminal. Kim et al. (55) harnessed kirigami-cut PVDF film for hand gesture recognition. Notably, according to the cutting direction and pattern on the film, the sensitivity, stretchability, hysteresis, and linearity can be adjusted for different purposes, as described in **Figure 2e** (55). Other diverse kinds of materials including piezoelectric NP-doped hydrogels (73, 74) and piezoelectric NWs (75) have also been adopted for wearable mechanical sensing applications.

In addition to noninvasive wearable mechanical sensors, implantable devices for decoding internal tissue biomechanics have gained significant interest. The most basic method is utilizing similar mechanical sensors on internal tissues with an encapsulation. For example, Dagdeviren et al. (76) harnessed thin PZT film for implantable gastrointestinal motility sensing. By adopting

PI encapsulation, the device showed adequate biocompatibility in cell culture tests, which suggests its feasibility for implantable applications. In vivo evaluation showed that the sensor could decode the volume variation of the stomach in a swine model. Another popular application of implantable mechanical sensing is cochlear implants, which utilize a piezoelectric sensor for acoustic sensing. İlik et al. (61) demonstrated a PZT-based thin film sensor with different lengths to decode acoustic waves with different frequencies for effective cochlear function.

Polymer-based piezoelectric materials have also been utilized for implantable devices. Wang et al. (53) developed a PVDF-based tissue-adhesive soft sensor for implantable blood pressure monitoring attached to the carotid artery. Acquired voltage output signals were effectively utilized for analyzing blood pressure, heart rate, and respiratory rate. Moreover, a fiber-based piezoelectric polymer was harnessed for implantable mechanical sensors by virtue of its high flexibility. For instance, electrospun PVDF-based arterial pressure sensors were successfully operated on carotid arteries, as described in **Figure 2f** (77). The monitoring was successfully conducted in vivo for an extended period of 10 weeks, during which the adolescent rat matured into adulthood and the artery continued to grow in size. Despite the increasing size of the artery with age, the device could operate successfully, which demonstrated the effectiveness of the flexible fiber-based piezoelectric mechanical sensor.

For implantable devices, biodegradability is one of the important requirements to minimize the required surgery. In that sense, biodegradable piezoelectric mechanical sensors also have been investigated. Various biodegradable materials have shown piezoelectric properties. For instance, poly-L-lactide (PLLA) polymer, which is biocompatible, biodegradable, and shows piezoelectric behavior, has been widely investigated for implantable mechanical sensor applications. Curry et al. (78) employed various US Food and Drug Administration–approved biocompatible materials including PLLA, molybdenum, and polylactic acid to fabricate an implantable force sensor for diaphragm pressure measurement. In addition, similar to the wearable PVDF-based polymer mechanical sensor, PLLA can also implement a doping strategy with inorganic piezoelectric NPs to enhance its piezoelectric sensitivity. For example, Shan et al. (79) doped BTO in PLLA fibers for evaluation of motor function during injury recovery by implanting the device on the leg of a rat with sciatic nerve injury, as described in **Figure 2g**. The output voltage signal exhibited high conformity when compared with that of a traditional electromyography-based muscle movement sensing signal, demonstrating the effectiveness of implantable motion recognition based on implantable piezoelectric mechanical sensors.

Suggested approaches for using piezoelectric materials for conformable mechanical sensing have shown high versatility and effectiveness for diverse biomedical applications. Furthermore, the development of novel biocompatible materials with high  $d$  and enhanced user comfort and flexibility—such as sweat-permeable three-dimensional piezoelectric fabrics—would be an effective approach for daily wearable applications (80), and creative device design for multiparameter sensing, such as multimodal sensors that could decode both strain and pressure, would be expected to allow for various other applications (81).

### 2.3. Neurostimulation

Neurostimulation is a promising tool for neurodegenerative diseases, visual restoration, and organ (liver, spleen, etc.) neuromodulation. There are various methodologies for neurostimulation, utilizing electrical, optical, chemical, and ultrasound-based techniques (82–86). Electrical stimulation is the most commonly used stimulation method, but implantable forms are necessary for deep organ stimulation (87, 88). Implanted devices for electrical stimulation usually suffer from biofouling and corrosion, which limit their operating lifetime. Optogenetics is also a promising

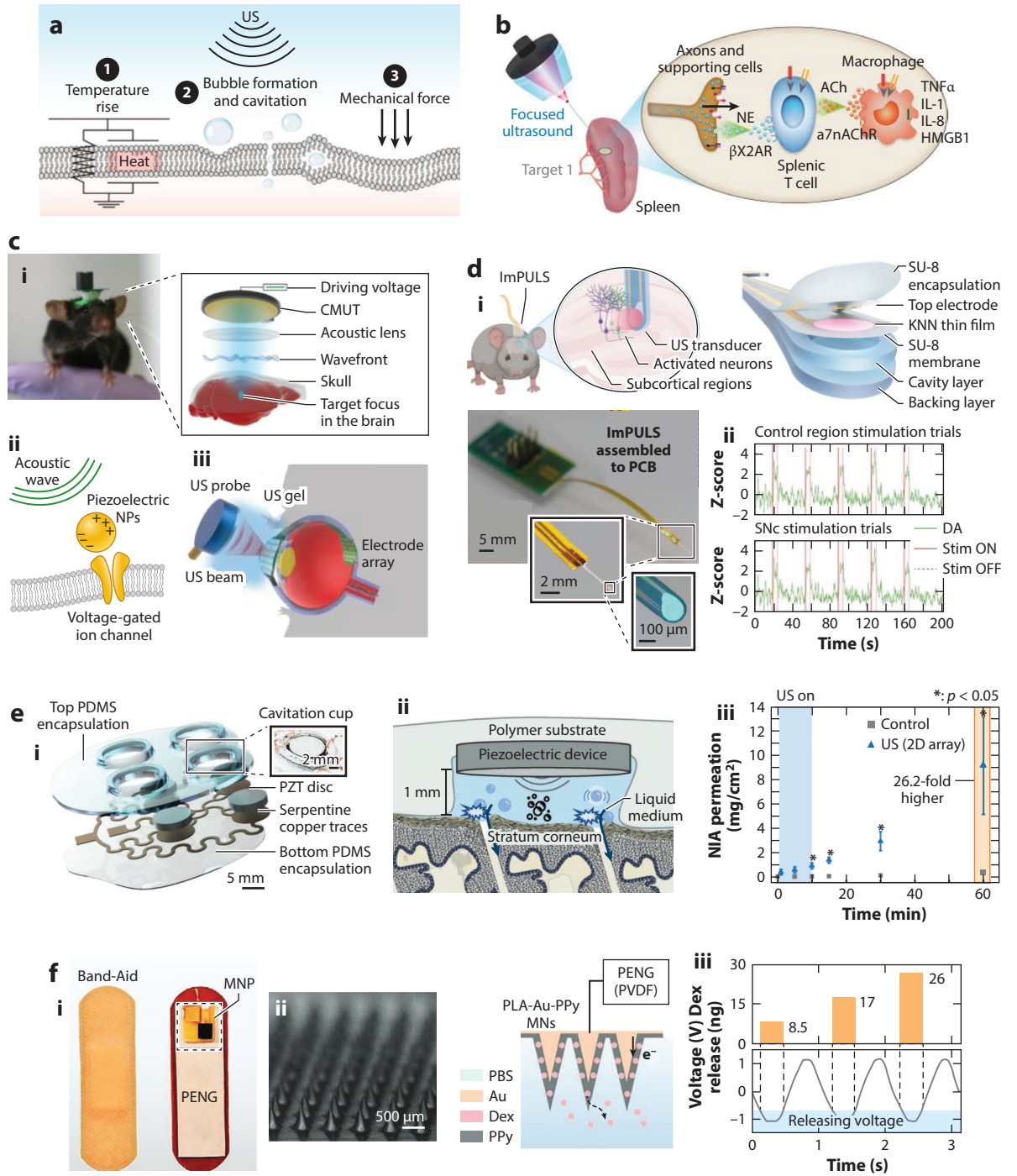
candidate for deep organ neurostimulation owing to its minimal invasiveness and high spatial resolution. However, to perform optogenetic treatment, local or systemic viral infection to deliver light-responsive opsin to the nervous system is required. This might pose the risk of immunogenicity and long-term safety issues (89). In contrast, ultrasound-based neurostimulation can be noninvasive and fully encapsulated and does not require any genetic modification (90, 91). Although noninvasive transcranial focused ultrasound can be affected by significant attenuation and target offset owing to the skull's high acoustic impedance, the selection of optimal operation frequency of the transducer (less than 1 MHz) and adoption of a phased array transducer and acoustic lens enable delivery of a focused ultrasound beam to target regions with a minimal energy loss (92–94).

Although there are numerous advantages of ultrasound-based neurostimulation, its exact mechanisms for the stimulation of neurons are still unclear. Several hypotheses for ultrasound-based neurostimulation are described in **Figure 3a** (91). When the acoustic wave generated by the ultrasound transducers reaches the neurons, several physical phenomena can happen: (a) temperature increase, (b) bubble formation and cavitation, and (c) acoustic radiation force (91). Among these phenomena, the thermal effect has a negligible effect on neurostimulation since low-intensity (less than 500 mW/cm<sup>2</sup>) ultrasound waves do not induce the hyperthermia effect, which is also known to induce activation of neurons (16). Another physical phenomenon that can occur is cavity formation using low-frequency ultrasound waves. Generated air bubbles can collide with the lipid bilayer membrane, even collapsing within the tissue, which induces the stimulation of the neurons by deforming the cell membrane (90).

The most widely accepted potential mechanism is the acoustic radiation force (91). The continuous acoustic pressure induced on the target neuron can deform (stretch and bend) the cell membrane, which can cause electrical potential change and activation of mechanosensitive ion channels (90). It was proposed that the deformation of the lipid bilayer cell membrane can generate membrane polarization, caused by a flexoelectric effect (95). Several studies have shown that the neurons are sensitive to mechanical stress. Recent studies have shown that ultrasound can directly activate several mechanosensitive ion channels [K<sup>+</sup> channel family TREK-1, TREK-2, and TRAAK; voltage-gated Na<sup>+</sup> and Ca<sup>2+</sup>; and piezo-type mechanosensitive channels (Piezo1 and Piezo2)] (96–100). Hence, ultrasound-based neurostimulation has potential for the treatment of neurodegenerative diseases.

Ultrasound neurostimulation is a useful tool not only for the brain but also for other body parts and internal organs such as the retina, liver, and spleen. Stimulating the nervous system in internal organs with high selectivity is challenging with electrical stimulation due to its tightly bundled nerve structure. However, ultrasound-based stimulation can achieve such high resolution through beam focusing, which converges the generated ultrasound beam into a single focal point (86). Hence, ultrasound can be an optimal solution. For instance, Cotero et al. (86) reported that focused ultrasound neurostimulation could regulate blood glucose levels by stimulating neurons within the spleen and liver, as shown in **Figure 3b**.

For ultrasound-based neurostimulation to be implemented for practical applications in the future, the development of ultrasonic transducers with a wearable form factor is required. Capacitive micromachined ultrasonic transducers (CMUTs) and piezoelectric micromachined ultrasonic transducers (PMUTs) fabricated on a flexible substrate or Si wafer are utilized for wearable transcranial focused ultrasound stimulation (101, 102). To generate focused ultrasound waves, an acoustic lens is incorporated in front of the transducers (shown in **Figure 3c**) or a phased array transducer is utilized (94). Kook et al. (92) reported a lightweight (0.75 g) CMUT array for a mouse behavioral study. They used acoustic lenses to focus the ultrasound beam and found no significant change in mouse movement while attaching the device to the mouse head.



(Caption appears on following page)

**Figure 3** (Figure appears on preceding page)

Neurostimulation and drug delivery. (a) Potential mechanisms of US-based neurostimulation. (b) Focused US enables local stimulation of spleen for glucose level regulation by beam focusing method. (c) Neurostimulation by CMUTs and acoustic lens for focused US generation with wearable form factor (i), remote neurostimulation by the electrical field formed by injected piezoelectric NPs (ii), and electrical retina stimulation by wireless activation of piezoelectric receiver arrays using ultrasonic transducer (iii). (d) Implantable KNN-based deep brain stimulation device (i) for dopamine release modulation (ii). (e) PZT-based wearable patch for transdermal niacinamide delivery (i). The converse piezoelectric effect formulates cavity bubbles, which can stimulate the stratum corneum (ii) to enhance drug permeation through the skin (iii). (f) MN-based transcutaneous Dex delivery device (i) operated by the direct piezoelectric effect from a connected PENG (ii). The drug release rate can be controlled by the electrical signal from the PENG, inducing reduction/oxidation of PPy (iii). Abbreviations: Ach, acetylcholine;  $\beta$ X2AR,  $\beta$ 2-adrenergic receptors; CMUT, capacitive micromachined ultrasonic transducer; DA, dopamine; Dex, dexamethasone; HMGB1, high mobility group box 1; IL, interleukin; ImPULS, implantable piezoelectric ultrasound stimulator; KNN,  $K_{1/2}Na_{1/2}NbO_3$ ; MN, microneedle; MNP, microneedle patch; NE, norepinephrine; NIA, niacinamide; NP, nanoparticle; PBS, phosphate buffer solution; PCB, printed circuit board; PDMS, polydimethylsiloxane; PENG, piezoelectric nanogenerator; PLA, polylactic acid; PPy, polypyrrole; PVDF, poly(vinylidene fluoride); PZT, lead zirconate titanate; SNc, substantia nigra pars compacta; stim, stimulation; TNF, tumor necrosis factor; US, ultrasound. Panel a adapted from Reference 91 (CC BY 4.0). Panel b adapted from Reference 86 with permission from Springer Nature. Panel c, subpanel i adapted from Reference 92 with permission from Springer Nature. Panel c, subpanel ii adapted from Reference 103 (CC BY 4.0). Panel c, subpanel iii adapted from Reference 104 (CC BY 4.0). Panel d adapted from Reference 83 with permission from Springer Nature. Panel e adapted from Reference 17 with permission from Wiley-VCH. Panel f adapted from Reference 133 with permission from Wiley-VCH.

Indirect approaches based on ultrasound neurostimulation are also widely utilized tools (103). By integrating piezoelectric receiver arrays and electrical stimulating electrodes, controlled, wireless activation of retinal stimulation by external ultrasound signals was demonstrated by Jiang et al. (104), as shown in **Figure 3c**. Various implantable piezoelectric nanomaterials including BTO NPs and PVDF nanosheets can be utilized for wireless stimulation of neurons by an electrical field generated from ultrasound waves transmitted remotely, as shown in **Figure 3c** (103).

To cope with the limitations of transcranial ultrasound neurostimulation, implantable ultrasonic transducers also have been reported for delivering acoustic energy directly and precisely to deep brain regions. Implantable ultrasound probes can be completely encapsulated, which could minimize the possibility of biofouling and corrosion of active layers (83). Recently, Hou et al. (83) reported highly flexible PMUT-based ultrasound transducers for deep brain stimulation, as shown in **Figure 3d**. They used biocompatible KNN as the piezoelectric layer and a biocompatible polymer (SU-8) as the encapsulation layer. They showed that ultrasound stimulation using an implantable PMUT could modulate dopamine release by stimulating neurons of the substantia nigra pars compacta to innervate the dorsal striatum, as shown in **Figure 3d** (83).

Ultrasound-based neurostimulation is a promising tool for the treatment of various neurodegenerative diseases with minimal invasiveness. To make ultrasound-based neurostimulation a universal tool for practical treatment, more clinical data need to be collected to establish detailed protocols, since ultrasound neurostimulation in humans is a very new methodology (18).

## 2.4. Drug Delivery

Piezoelectric materials have the potential to enable efficient drug delivery through the utilization of their piezoelectric effect to induce stimulation for drug delivery (17, 105). Among various biomedical applications, drug delivery has gained substantial interest due to its potential to provide various kinds of therapeutic substances to target tissues (106–108). The application comprises cosmetic use (17, 105), clinical therapy (109–112), and neural function modulation (113). The therapeutic benefit of drugs is critically correlated with the method of drug delivery within the body (106); thus, various strategies for drug delivery aimed at various target tissues have been vigorously

investigated (107, 114–117). Here, we demonstrate representative piezoelectric material-based drug delivery applications from wearable devices.

Transdermal drug delivery is a simple but efficient method for providing a steady supply of a drug in a noninvasive way (118, 119). The method is more convenient than a typical venous injection of a drug because it does not require assistance from professionals nor invasive operation. Moreover, various drugs including hyaluronic acid (105), fentanyl (120), caffeine (120), niacinamide (17), and insulin (121) have been able to be applied directly on the skin for transdermal drug absorption. However, since human skin has multiple barrier layers that protect against the penetration of external substances, the permeability of the skin is generally not high enough for typical passive transdermal drug delivery (122). In this regard, various methods including iontophoresis (123), electroporation (124), sonophoresis (125), thermal enhancers (126), and chemical enhancers (127) have been adopted to promote drug delivery through the skin.

Among these approaches, sonophoresis utilizing piezoelectric material as a mechanical stimulator has exhibited significant performance improvements in transdermal drug delivery, in terms of the drug absorption speed through the skin (128, 129). By utilizing the converse piezoelectric effect, when voltage is applied to the piezoelectric material, ultrasound waves are induced from the mechanical vibration of the piezoelectric material. The main principle of sonophoresis is based on the cavitation effect induced by ultrasound waves (130). When the piezoelectric material interfaces with the skin through the fluid medium between them, the ultrasound from the piezoelectric material induces cavitation bubbles. The cavity can stimulate the stratum corneum to make openings between skin cells, such that the skin becomes more permeable to the drug (130). The main advantage of sonophoresis is the ability to adjust the cavitation mechanism by modulating the frequency and voltage of the input sinusoidal electrical signal (17). Cavitation mechanisms of sonophoresis differ as a function of the frequency of the ultrasound (118). When high-frequency ultrasound is applied ( $>0.7$  MHz), the radius of the cavity becomes small, and the size becomes similar to the distance between each cell in the stratum corneum (17). In this case, the effect occurs in the skin, whereas low-frequency ultrasound (20–100 kHz) acts at the skin surface (118). Low-frequency stimulation formulates larger cavity bubbles and induces various transient effects including shockwave generation and bubble collapse (118). When a higher voltage is applied to the piezoelectric material, the pressure within the fluid increases. A certain level of threshold voltage is needed for cavitation formation with adequate pressure (17). Generally, higher voltage produces more cavities, which creates more frequent cavitation effects (118).

Yu et al. (17) developed a conformable transdermal drug delivery patch utilizing PZT as the piezoelectric material and niacinamide as the drug. They successfully confirmed the effect of the ultrasound induced by the piezoelectric material, by exhibiting a higher niacinamide permeation amount compared with normal passive permeation, as demonstrated in **Figure 3e**. The cumulative niacinamide permeation was 26.2-fold higher ( $9.14 \pm 4.00$  mg/cm<sup>2</sup>) when utilizing an ultrasound patch compared with the permeation rate without the device ( $0.35 \pm 0.09$  mg/cm<sup>2</sup>) after 1 h of operation on porcine skin. Li et al. (105) introduced a sonophoresis face mask promoting the delivery of hyaluronic acid, which gives the skin more moisture. The sonophoresis mask induced a relatively higher permeation speed at shallow depths from the skin surface than in deep tissue. Moreover, the drug permeation using the ultrasound mask was higher than that of the thermal treatment group, which applied heat, and the control group, which utilized passive transdermal drug delivery, over a 30- $\mu$ m depth from the skin surface. Such results demonstrate that wearable ultrasound stimulation devices can effectively enhance transdermal drug delivery.

In addition to conventional noninvasive transdermal drug delivery, a method of harnessing microneedles in wearable form that can contain drugs in the cones and penetrate them into skin tissues has been on the rise (131, 132). Such a method enables penetration of the drug to the deep

target tissues, passing over the relatively impermeable stratum corneum. However, one of the most important functions of microneedle-based drug delivery systems is the ability to control the release rate of the drug (133). To enable drug dose control, diverse external sources to modulate the drug release have been devised. Among them, piezoelectric material-based drug release methods have shown not only enhanced drug delivery efficiency but also precise control over drug release by utilizing either direct or converse piezoelectric effects.

Drug release rates can be precisely controlled by utilizing the electrical voltage and current generated from the direct piezoelectric effect. For instance, Yang and colleagues (133, 134) developed a self-powered controllable microneedle-based drug delivery system, as demonstrated in **Figure 3f**. The microneedle of the device was fabricated with the conductive polymer polypyrrole (PPy), which can efficiently load and release various drugs by switching between its oxidative and reductive states. When external electrical stimulation is applied to PPy, oxidation and reduction induce the movement of ions and water into and out of the polymer, and the reaction accompanies the shrinking and expanding of the polymer microneedle. Therefore, the release rate of the drug can be properly controlled by adjusting applied electrical signals to the PPy. For electrical stimulation, piezoelectric nanogenerators (PENGs) were adopted. Compared with no stimulation, the drug release efficiency was fourfold higher (~80%) when utilizing piezoelectric stimulation (~20%) after 180 min of operation (133). As PENGs can transduce mechanical energy collected from the motion of the body including joint movements and heartbeats, the device can be operated in a self-powered manner. The PENG was composed of PVDF polymer to create a flexible form factor. The device could release 8.5 ng of dexamethasone per electrical stimulation induced from the AC signals generated by the PENG (133). An *in vivo* rat experiment demonstrated that the controlled drug release from the device showed effective treatment of psoriasis.

Similar to the noninvasive approach mentioned above, mechanical activation of a microneedle drug carrier by the converse piezoelectric effect can also control the drug release rate. For instance, Wu et al. (134) fabricated microneedles with biocompatible light-responsive resin through 3D printing, which were able to load 400  $\mu\text{L}$  of drugs in a connected liquid reservoir. On the drug reservoir, PZT was attached to generate acoustic streaming for drug release. When electrical signals were applied to the PZT material, the acoustic waves generated from the converse piezoelectric effect oscillated the microneedle. The oscillation produced a streaming vortex at the tip of each microneedle, which extracted drugs from the microneedle. By adjusting the power of the acoustic wave, the drug release rate could be modulated according to the user's need. Overall, the injected volume and absorbance of the drug showed a linear relationship (40  $\mu\text{L}/\text{min}$  at 4 W) (134). Furthermore, multiple mechanisms including cavitation, sonophoresis, thermal effects, and radiation pressure effects were concurrently observed during acoustic stimulation, which helped increase the permeation of the drugs for more efficient drug delivery. The researchers exhibited controllable drug delivery with mouse experiments by delivering sodium fluorescein with the microneedle device. The *in vivo* experiment also validated the controllable drug release of the device by exhibiting a linear relationship between the delivered drug concentration with applied power and operation time. As this method can harness various liquid-based drugs for delivery, it is expected to be adopted for various transcutaneous drug delivery applications.

In summary, wearable and implantable technology utilizing piezoelectric-induced ultrasound is expected to create novel clinical solutions for efficient drug delivery. In addition to drug delivery through the skin, drug delivery methods targeting deeper tissue regions are also being investigated. For instance, the injection of NPs or microbubbles could be enhanced by applying ultrasound stimulation, showing its potential for tumor therapy (135).

## 2.5. Ultrasound Imaging

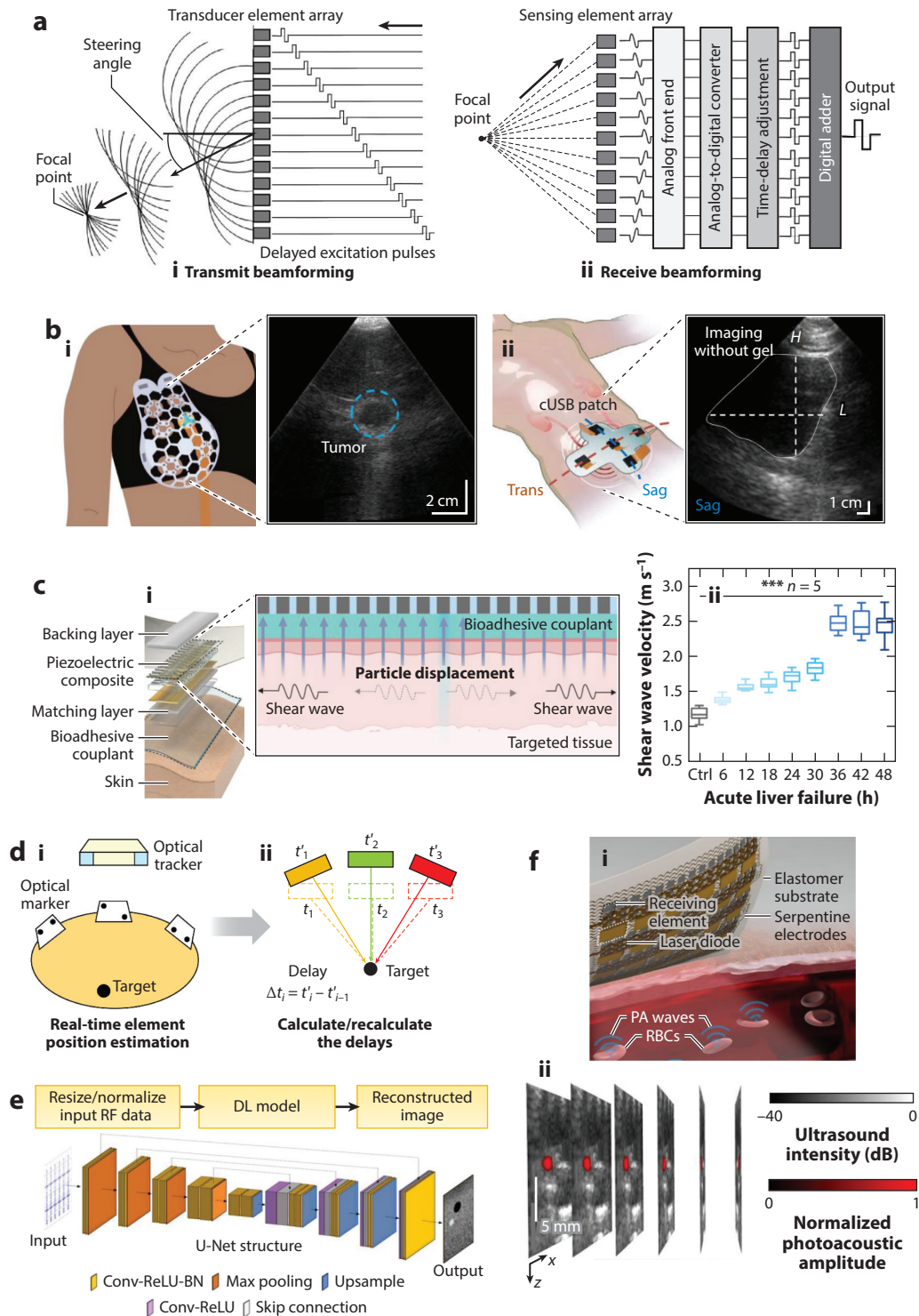
Ultrasound imaging, or sonography, works on the principles of sound wave reflection and transmission, typically operating at frequencies higher than 20,000 Hz. These high-frequency vibrations, also known as ultrasound waves, are emitted by a transducer based on the converse piezoelectric effect, as shown in **Figure 1**. When these transducers are activated on the surface of the skin to be examined, generated ultrasound waves propagate through the skin and encounter various tissues and structures. During the propagation, partial reflection of ultrasound waves at each interface might occur due to different densities of the biological mediums (bone, blood, muscle, etc.) (136). When the reflected waves arrive at the receiving transducers, the transducers convert the ultrasound waves back into electrical signals by the direct piezoelectric effect, as shown in **Figure 1**. These signals are then denoised and converted into digital samples by the analog front end for further processing. The time it takes for the sound waves to return and the intensity of the reflected ultrasound wave can help determine the location and nature of the structures being examined. The image reconstruction algorithm, commonly known as the beamforming algorithm, utilizes this information to create a visual image of the internal structure (14). This allows for real-time imaging of organs, tissues, and blood flow, making it a viable alternative to delayed imaging techniques such as magnetic resonance imaging.

Although ultrasound waves could have potentially harmful bioeffects, they are safer than imaging techniques using ionizing radiation such as X-rays. Safety in ultrasound diagnostics is ensured by regulating temperature and pressure limits, using indices (e.g., thermal index, mechanical index) for risk estimation, and adhering to regulatory guidelines set by regulatory bodies (137). Ultrasound imaging is notably more portable than most other imaging tools, allowing for convenient bedside and field use.

In this section, the brief working principles of piezoelectric transducers for ultrasound imaging, different imaging modes, design strategies for imaging systems, and their applications are discussed. Piezoelectric transducers are at the very heart of any ultrasound imaging system. Single-element transducers consist of a single piezoelectric element and are typically used in applications where lower dimensionality is acceptable (138), due to the lack of focusing and beam steering capabilities. They generally require movement from the operator to scan a 2D area, but recent works have explored and demonstrated that an acoustic lens could be utilized for dynamic beam focusing (139). Yin et al. (139) demonstrated that by exploiting an acoustic lens composed of randomly distributed scatters, high-order multiple scattering of ultrasound waves could be achieved. Based on this, dynamic focusing could be achieved using a single transducer by manipulating the transmitting waveform.

Array-based multielement transducers offer a large improvement in imaging capabilities, especially resolution and field of view. As shown in **Figure 4a**, phased array ultrasound transducers could utilize delayed voltage pulses to drive each transducer element to modulate the focal point, which is called beam steering (140). This capability allows for precise spatial focusing and higher quality image rendering. The complexity of controlling numerous elements requires the development of complex beamforming algorithms.

There are various imaging modes that can be utilized by ultrasound transducers. Among them, the most commonly used imaging mode is the brightness mode, or B-mode, which generally uses multielement transducers in a 1D array form. It produces a 2D grayscale image where each pixel value (brightness) represents the intensity of the reflected acoustic wave. The depth (vertical axis of the image) of the interface can be interpreted from the time at which the reflected wave returns to the transducer, and the lateral information (horizontal axis of the image) is inferred from the specific geometric location of the piezoelectric element receiving the signal (141). B-mode is widely



(Caption appears on following page)

**Figure 4** (Figure appears on preceding page)

Ultrasound imaging. (a) Principle of transmit (*i*) and receive (*ii*) beamforming with ultrasound transducing element array. (b) Wearable ultrasound imaging devices for breast tumor detection (*i*) and bladder volume monitoring (*ii*). (c) Wearable bioadhesive ultrasound device (*i*) for acute liver failure detection with shear wave elastography method. The progression of the acute liver failure can be estimated through the shear wave velocity measured from the device (*ii*). (d) Optical tracking method for beamforming on complex surfaces (*i*). The delay calculation can be adjusted according to the surface information acquired from the optical marker tracking (*ii*). (e) DL-based ultrasound image reconstruction method trained with RF data acquired from a single transducer element. (f) Wearable PA patch decoding ultrasound waves from RBCs, induced by laser pulse (*i*). The ultrasound wave enables 3D imaging of RBCs (*ii*). Abbreviations: BN: batch normalization; conv, convolution; Ctrl, control; cUSB, conformable ultrasound breast; DL, deep learning; PA, photoacoustic; RBC, red blood cell; ReLU, rectified linear unit; RF, radiofrequency; sag, sagittal; trans, transverse. Panel *a* (left) adapted from Reference 140 (CC-BY 4.0). Panel *b* (left) adapted from Reference 15 with permission from American Association for the Advancement of Science. Panel *b* (right) adapted from Reference 146 with permission from Springer Nature. Panel *c* adapted from Reference 147 with permission from American Association for the Advancement of Science. Panel *e* adapted from Reference 152 with permission from IEEE. Panel *f* adapted from Reference 155 with permission from Springer Nature.

used for anatomical imaging, enabling visualization of organs, muscles, and fetuses during pregnancy. Its advantages include providing clear structural information and guiding interventional procedures such as biopsies.

3D B-mode imaging can be performed with the help of 2D transducer arrays, where, similar to the above method, the image is generated with two dimensions other than depth derived from the geometrical 2D location of the element in consideration, and the pixel value (brightness) continues to represent the intensity of the reflected acoustic wave (142). The motion mode, or M-mode, displays a single scan (multiple frames) over time representing motion in the field of view. This is very useful in cardiac imaging where the movement of valves, walls, and arteries can be selectively monitored given the high spatiotemporal resolution of ultrasound imaging today (143). Doppler mode leverages the Doppler effect, where the frequency of the ultrasound waves is shifted due to the motion of the reflecting surface, such as blood vessels. This shift in frequency can then be processed by the imaging system to decode the speed and direction of motion, and the spatial information can be retrieved as in B-mode imaging. Doppler ultrasound is crucial for assessing vascular conditions, detecting blockages, and evaluating cardiac function. Its primary advantage is real-time visualization of blood flow dynamics, aiding in diagnosing circulatory issues (144).

A wearable and continuous ultrasound imaging system is essential for real-time and continuous health monitoring, enabling chronic disease management, point-of-care assessment, and early disease detection.

Wearable ultrasound imaging devices are typically made up of a piezoelectric transducer for actuation and reception, the transmission circuitry to control the actuation, the analog front end for reception of the reflected acoustic waves, a processor for beamforming, and wireless communication to relay the information to the user, as shown in **Figure 4a** (145). Interfacing the transducer with the skin should be conformal to ensure seamless application and avoid air gaps in the transducer–skin interface. This results in better comfort for long-term use as well. Given the complexity of ultrasound imaging and the high-performance requirements of the transducer, creating a flexible transducer that is comparable to rigid transducer performance is challenging due to the need to balance mechanical flexibility with efficient mechanical-to-electrical signal conversion. The current research trends of wearable ultrasound imaging systems mainly focus on the development of conformable and wearable ultrasound transducers, and other peripheral electronics mentioned above rely on bulky commercial ultrasound systems such as GE and Verasonics systems. Such limitations should be addressed to realize fully wearable ultrasound imaging systems. In this section, we address some state-of-the-art wearable ultrasonic transducers for various imaging technologies and fully integrated ultrasound imaging systems, along with their challenges and future directions.

Du et al. (15) demonstrated a wearable ultrasound imager designed for deep tissue scanning of the breast, aimed at applications such as breast tumor detection, as shown in **Figure 4b**. The 64-element 1D rigid transducer array operating at 7 MHz was developed using a Yb/Bi-doped  $\text{Pb}(\text{In}_{1/2}\text{Nb}_{1/2})\text{O}_3$ -PMN-PT (PIN-PMN-PT) single crystal. The device features a conformable honeycomb structure clipped onto a soft bra. This structure allows for free movement of the transducer on the breast surface and has a locking mechanism in place for reliable continuous monitoring in a specific position (15). Zhang et al. (146) developed a flexible patch-based ultrasound device for bladder volume monitoring, as shown in **Figure 4b**. This work demonstrated successful continuous monitoring without the use of ultrasound coupling gel, which evaporates and needs frequent replacement, posing an inconvenience for a wearable use scenario (146). The bladder volume monitoring patch uses a 64-array transducer made from Sm/La-doped PMN-PT. It operates at  $\sim 2$ –5 MHz, allowing for deeper penetration capability compared with the breast patch. Given the large field of view required for bladder monitoring, the device was designed with multiple rigid phased array transducers placed onto a common conformable substrate made of silicone rubber. This prevents the degradation of image resolution while allowing a larger field of view, ensuring reliable volume monitoring (146). Both of these devices use rigid transducer arrays paired with a conformal substrate/structure to interface effectively with the human body.

Developing highly adhesive interface materials between rigid ultrasound transducer arrays and the skin is critical for long-term ultrasound imaging. Wang and colleagues (147, 148) reported on a hydrogel-based bioadhesive material with high interfacial toughness and low acoustic attenuation, suitable for long-term wearable ultrasound imaging. Liu et al. (147) applied this bioadhesive layer to wearable ultrasound shear wave elastography for long-term (more than 48 h) liver monitoring in a mouse model, as shown in **Figure 4c**. Ultrasound shear wave elastography is one of the ultrasound-based imaging methods that monitors tissue elasticity (shear modulus) (149). It utilizes multiple high-intensity ultrasound waves directed at the target area to create shear waves that propagate through the liver. Afterward, the same transducer performs three-plane wave compounding at the same operating frequency to detect particle displacement (147). These displacements and their frequencies are geometrically mapped to assess tissue stiffness (147). By measuring the speed at which these waves travel through various tissue sections, this technique provides critical insights into the liver's condition, making it indispensable for functional monitoring.

The methods mentioned earlier provide unique approaches for applying rigid transducers to soft body tissues for imaging. These devices have limited apertures and are applied to typically flat and stable surfaces, making it feasible to calculate delays accurately for reliable image reconstruction. However, when the transducer geometry (curvature and spacing between elements) changes dynamically by the skin deformation, signal timing for beam steering and beamforming for image reconstruction becomes extremely complicated. In **Figure 4d,e**, two methods for image reconstruction when transducer geometry is changing are shown. The method highlighted in **Figure 4d** tracks the geometries of multiple elements optically. This information is used to calculate precise delays for beamforming and accurately reconstruct the image (150). **Figure 4e** demonstrates the use of artificial intelligence (AI) for beamforming in flexible transducers. A U-Net deep learning model was trained from prebeamformed RF data with corresponding ultrasound images reconstructed from a conventional delay-and-sum process and geometric phase correction. This approach enabled effective image reconstruction from the input RF data, producing images with high contrast and low variability (151, 152). Alternatively, shape estimation algorithms have been proposed for beamforming correction, but they often fail due to their large latencies and the significant processing power required. There remains a significant need for solutions that enable reliable image rendering for soft ultrasound transducers.

Apart from conventional ultrasound-based imaging, photoacoustic imaging is another methodology that combines electromagnetic radiation with ultrasound transducers to image internal tissues (153). Photoacoustic imaging has several advantages over conventional ultrasound imaging including high spatial resolution and multiple functional imaging capabilities (vascular structure, blood oxygenation, and endogenous molecules) (153). In photoacoustic imaging, laser diodes with visible to near-infrared wavelengths are utilized for a light source to obtain several centimeters of penetration depth (153). When internal tissues interact with the incident light, they undergo thermoelastic expansion, generating acoustic waves (154). These waves are then captured by the piezoelectric transducers, enabling high-resolution imaging (155). This entire process of converting light-induced acoustic signals into detailed images is the core of photoacoustic imaging. Gao et al. (155) proposed a conformable photoacoustic patch integrating a surface-emitting laser and ultrasound transducers, as shown in **Figure 4f**. Using this device, they could image hemoglobin dynamics with a penetration depth of 2 cm (155).

Most existing ultrasound imaging devices utilize large, bulky, and expensive ultrasound imaging systems (e.g., Verasonics and GE Logiq), which are impractical for wearable and long-term applications. Hence, beyond the development of conformable ultrasound transducers, endeavors to develop wearable ultrasound imaging systems should be pursued as well (148, 155). Lin et al. (145) developed the first fully integrated wearable ultrasound imaging system for deep-tissue monitoring that supports multiple modes of imaging. This device performed image reconstruction and digital processing of the RF data (which was transmitted via Wi-Fi to a mobile device), drastically reducing the power and processing requirements of the wearable patch. The study demonstrated successful continuous monitoring of central blood pressure, heart rate, and cardiac output for up to 12 h (145).

Ultrasound imaging has proven to be a powerful tool for monitoring internal tissues and organs for various purposes. Imaging methods such as shear wave elastography and photoacoustic imaging could offer various functions that cannot be achieved by conventional ultrasound imaging. Further advancements in fully flexible transducers, their imaging algorithms, and high-performance portable ultrasound imaging systems are required to make ultrasound imaging widely available outside of medical institutions at a low cost.

### 3. CONCLUSION AND OUTLOOKS

Piezoelectric materials have been widely investigated for various wearable devices in biomedical fields. In this review, we provide a comprehensive overview of wearable and implantable piezoelectric devices for various applications. Owing to their unique electromechanical transduction properties, piezoelectric materials can be utilized for multiple purposes including mechanical sensing, energy harvesting, drug delivery, neurostimulation, and ultrasound imaging. In this review, we address the basic working mechanisms of piezoelectric devices for the target applications and provide material and device design strategies for high-performance, flexible, and conformable form factors.

Although all of the applications discussed in this review are highly promising and could evolve into wearable and implantable form factors, there are several challenges that should be addressed for further development and commercialization.

1. Improvement of the performance of piezoelectric-based devices: Although there has been great progress in piezoelectric material-based wearable and implantable devices, the devices themselves still need to be further improved for real applications. For instance, wearable sensors based on piezoelectric materials need to be more sensitive and conformable to

properly integrate with soft biological tissues. The Young's modulus of biological tissues is usually less than 10 MPa (156), whereas most piezoelectric materials, even those based on organics, have a Young's modulus higher than 1 GPa (approximately 5 GPa for PVDF and 70 GPa for PZT, respectively) (157). Such a large difference in Young's modulus could result in poor conformal contact, user discomfort, and delamination. Wearable energy harvesters should have higher power conversion efficiency and improved structures to effectively harvest the energy from body motions with a low operation frequency. For wearable ultrasound transducers for imaging, image resolution should be improved and image reconstruction algorithms need to be enhanced to compensate for the deformation of the transducers conformably attached to the skin surface.

2. Development of data acquisition system: Most currently reported wearable biomedical devices are connected with external electronics by an external cable. Such an external connection is not practical for wearable devices. Hence, a portable system with reading and control circuits for wearable devices, wireless communication, and power management is required for wearable electronics to be completely wireless and cable-free.
3. Development of closed-loop feedback system: Ideal wearable biomedical devices should be capable of sensing biomarkers and performing activities/treatments based on the readings acquired from the sensors. As discussed above, wearable devices based on piezoelectric materials can perform multiple biomedical activities from sensing to treatment. Hence, the development of closed-loop systems addressing both sensing and treatment responses based on piezoelectric devices could be one of the potential applications of wearable piezoelectronic devices.
4. Integration with AI and big data analysis: Owing to the recent advancement of AI, data collected from wearable devices have become highly promising for more accurate disease diagnosis and classification. Hence, machine learning (ML) algorithms can be developed to utilize the data collected from wearable piezoelectric devices. Such ML algorithms can be applied for motion detection, tumor recognition, and so forth. With rising model complexities, it is essential to explore low-resource ML techniques for on-device inferencing. Currently, cloud-based inferencing helps address the issue but fails to provide real-time output. In the future, on-device learning and classification are also necessary to ensure the privacy of personal medical data.

Wearable piezoelectric devices hold significant promise not only in the biomedical field but also in various areas including general healthcare, the Internet of Things, augmented and virtual reality, and prosthetics.

## DISCLOSURE STATEMENT

The authors are not aware of any affiliations, memberships, funding, or financial holdings that might be perceived as affecting the objectivity of this review.

## ACKNOWLEDGMENTS

This work was supported by the National Science Foundation CARRER: Conformable Piezoelectrics for Soft Tissue Imaging (grant 2044688) award and MIT Media Lab Consortium funding. H.Y. acknowledges support from the Korean Government Scholarship Program for Study Overseas (KGSPSO) fellowship from the National Institute for International Education (NIIED), Korea.

## LITERATURE CITED

1. Thimbleby H. 2013. Technology and the future of healthcare. *J. Public Health Res.* 2:e28
2. Wamble DE, Ciarametaro M, Dubois R. 2019. The effect of medical technology innovations on patient outcomes, 1990–2015: results of a physician survey. *J. Manag. Care Spec. Pharm.* 25:66–71
3. Kasoju N, Remya NS, Sasi R, Sujesh S, Soman B, et al. 2023. Digital health: trends, opportunities and challenges in medical devices, pharma and bio-technology. *CSI Trans. ICT* 11:11–30
4. Fernandez SV, Sadat D, Tasnim F, Acosta D, Schwendeman L, et al. 2022. Ubiquitous conformable systems for imperceptible computing. *Foresight* 24:75–98
5. Blanc L, Delchambre A, Lambert P. 2017. Flexible medical devices: review of controllable stiffness solutions. *Actuators* 6:23
6. Wang L, Jiang K, Shen G. 2021. Wearable, implantable, and interventional medical devices based on smart electronic skins. *Adv. Mater. Technol.* 6:2100107
7. Agaronnik N, Campbell EG, Ressalam J, Jezzoni LI. 2019. Accessibility of medical diagnostic equipment for patients with disability: observations from physicians. *Arch. Phys. Med. Rehabil.* 100:2032–38
8. Yetisen AK, Martinez-Hurtado JL, Ünal B, Khademhosseini A, Butt H. 2018. Wearables in medicine. *Adv. Mater.* 30:1706910
9. Melodie C-G, Panpan L, Jeongjae R, Seungbum H. 2018. Piezoelectric materials for medical applications. In *Piezoelectricity*, ed. GV Savvas, M Dimitroula, Chapter 7. Rijeka, Croatia: IntechOpen
10. Zhang L, Du W, Kim J-H, Yu C-C, Dagdeviren C. 2024. An emerging era: conformable ultrasound electronics. *Adv. Mater.* 36:2307664
11. Dagdeviren C, Yang BD, Su Y, Tran PL, Joe P, et al. 2014. Conformal piezoelectric energy harvesting and storage from motions of the heart, lung, and diaphragm. *PNAS* 111:1927–32
12. Zhou H, Zhang Y, Qiu Y, Wu H, Qin W, et al. 2020. Stretchable piezoelectric energy harvesters and self-powered sensors for wearable and implantable devices. *Biosens. Bioelectron.* 168:112569
13. Panda S, Hajra S, Mistewicz K, In-na P, Sahu M, et al. 2022. Piezoelectric energy harvesting systems for biomedical applications. *Nano Energy* 100:107514
14. Wells PNT. 2006. Ultrasound imaging. *Phys. Med. Biol.* 51:R83
15. Du W, Zhang L, Suh E, Lin D, Marcus C, et al. 2023. Conformable ultrasound breast patch for deep tissue scanning and imaging. *Sci. Adv.* 9:eadh5325
16. Dalecki D. 2004. Mechanical bioeffects of ultrasound. *Annu. Rev. Biomed. Eng.* 6:229–48
17. Yu C-C, Shah A, Amiri N, Marcus C, Nayeem MOG, et al. 2023. A conformable ultrasound patch for cavitation-enhanced transdermal cosmeceutical delivery. *Adv. Mater.* 35:2300066
18. Beisteiner R, Hallett M, Lozano AM. 2023. Ultrasound neuromodulation as a new brain therapy. *Adv. Sci.* 10:2205634
19. Chorsi MT, Curry EJ, Chorsi HT, Das R, Baroody J, et al. 2019. Piezoelectric biomaterials for sensors and actuators. *Adv. Mater.* 31:1802084
20. Nwalike ED, Ibrahim KA, Crawley F, Qin Q, Luk P, Luo Z. 2023. Harnessing energy for wearables: a review of radio frequency energy harvesting technologies. *Energies* 16:5711
21. Ali A, Shaukat H, Bibi S, Altabay WA, Noori M, Kouritem SA. 2023. Recent progress in energy harvesting systems for wearable technology. *Energy Strat. Rev.* 49:101124
22. Choi Y-M, Lee MG, Jeon Y. 2017. Wearable biomechanical energy harvesting technologies. *Energies* 10:1483
23. Niu P, Chapman P, Riemer R, Zhang X. 2004. Evaluation of motions and actuation methods for biomechanical energy harvesting. In *Proc. 2004 IEEE 35th Annual Power Electronics Specialists Conference, Aachen, Germany, June 20–25, 2004, Volume 3*, pp. 2100–6. New York: IEEE
24. Xu C, Song Y, Han M, Zhang H. 2021. Portable and wearable self-powered systems based on emerging energy harvesting technology. *Microsyst. Nanoeng.* 7:25
25. Hwang G-T, Annapureddy V, Han JH, Joe DJ, Baek C, et al. 2016. Self-powered wireless sensor node enabled by an aerosol-deposited PZT flexible energy harvester. *Adv. Electron. Mater.* 6:1600237
26. Park K-I, Son JH, Hwang G-T, Jeong CK, Ryu J, et al. 2014. Highly-efficient, flexible piezoelectric PZT thin film nanogenerator on plastic substrates. *Adv. Mater.* 26:2514–20

27. Lu X, Qu H, Skorobogaty M. 2017. Piezoelectric microstructured fibers via drawing of multimaterial preforms. *Sci. Rep.* 7:2907
28. Su Y, Dagdeviren C, Li R. 2015. Measured output voltages of piezoelectric devices depend on the resistance of voltmeter. *Adv. Funct. Mater.* 25:5320–25
29. He Q, Briscoe J. 2024. Piezoelectric energy harvester technologies: synthesis, mechanisms, and multifunctional applications. *ACS Appl. Mater. Interfaces* 16:29491–520
30. Kanno I, Ichida T, Adachi K, Kotera H, Shibata K, Mishima T. 2012. Power-generation performance of lead-free (K,Na)NbO<sub>3</sub> piezoelectric thin-film energy harvesters. *Sens. Actuators A Phys.* 179:132–36
31. Hyeon DY, Park K-I. 2019. Piezoelectric flexible energy harvester based on BaTiO<sub>3</sub> thin film enabled by exfoliating the mica substrate. *Energy Technol.* 7:1900638
32. Peng R, Zhang B, Dong G, Wang Y, Yang G, et al. 2024. Enhanced piezoelectric energy harvester by employing freestanding single-crystal BaTiO<sub>3</sub> films in PVDF-TrFE based composites. *Adv. Funct. Mater.* 34:2316519
33. An J, Park H, Jung YH, Min S, Kim DH, et al. 2024. In vivo flexible energy harvesting on porcine heart via highly-piezoelectric PIN-PMN-PT single crystal. *Nano Energy* 121:109227
34. Kim DH, Shin HJ, Lee H, Jeong CK, Park H, et al. 2017. In vivo self-powered wireless transmission using biocompatible flexible energy harvesters. *Adv. Funct. Mater.* 27:1700341
35. Wyser Y, Pelletier C, Lange J. 2001. Predicting and determining the bending stiffness of thin films and laminates. *Packag. Technol. Sci.* 14:97–108
36. Li H, Lee HB, Kang J-W, Lim S. 2023. Three-dimensional polymer-nanoparticle-liquid ternary composite for ultrahigh augmentation of piezoelectric nanogenerators. *Nano Energy* 113:108576
37. Kim S-R, Yoo J-H, Kim JH, Cho YS, Park J-W. 2021. Mechanical and piezoelectric properties of surface modified (Na,K)NbO<sub>3</sub>-based nanoparticle-embedded piezoelectric polymer composite nanofibers for flexible piezoelectric nanogenerators. *Nano Energy* 79:105445
38. Wankhade SH, Tiwari S, Gaur A, Maiti P. 2020. PVDF-PZT nanohybrid based nanogenerator for energy harvesting applications. *Energy Rep.* 6:358–64
39. Baek C, Park H, Yun JH, Kim DK, Park K-I. 2017. Lead-free BaTiO<sub>3</sub> nanowire arrays-based piezoelectric energy harvester. *MRS Adv.* 2:3415–20
40. Koka A, Zhou Z, Sodano HA. 2014. Vertically aligned BaTiO<sub>3</sub> nanowire arrays for energy harvesting. *Energy Environ. Sci.* 7:288–96
41. Waseem A, Johar MA, Abdullah A, Bagal IV, Ha J-S, et al. 2021. Enhanced performance of a flexible and wearable piezoelectric nanogenerator using semi-insulating GaN:Mg/ZnO coaxial nanowires. *Nano Energy* 90:106552
42. Todaro MT, Guido F, Algieri L, Mastronardi VM, Desmaële D, et al. 2018. Biocompatible, flexible, and compliant energy harvesters based on piezoelectric thin films. *IEEE Trans. Nanotechnol.* 17:220–30
43. Petritz A, Karner-Petritz E, Uemura T, Schäffner P, Araki T, et al. 2021. Imperceptible energy harvesting device and biomedical sensor based on ultraflexible ferroelectric transducers and organic diodes. *Nat. Commun.* 12:2399
44. Kim S-R, Yoo J-H, Cho YS, Park J-W. 2019. Flexible piezoelectric energy generators based on P(VDF-TrFE) nanofibers. *Mater. Res. Express* 6:086311
45. Qin W, Zhou P, Xu X, Irshad MS, Qi Y, Zhang T. 2022. Enhanced output performance of piezoelectric energy harvester based on hierarchical Bi<sub>3.15</sub>Nd<sub>0.85</sub>Ti<sub>3</sub>O<sub>12</sub> microspheres/PVDF-HFP composite. *Sens. Actuators A Phys.* 333:113307
46. Zhao J, You Z. 2014. A shoe-embedded piezoelectric energy harvester for wearable sensors. *Sensors* 14:12497–510
47. Liu H, Zhong J, Lee C, Lee S-W, Lin L. 2018. A comprehensive review on piezoelectric energy harvesting technology: materials, mechanisms, and applications. *Appl. Phys. Rev.* 5:041306
48. Yang Y, Chen Z, Kuai Q, Liang J, Liu J, Zeng X. 2022. Circuit techniques for high efficiency piezoelectric energy harvesting. *Micromachines* 13:1044
49. Min S, Kim DH, Joe DJ, Kim BW, Jung YH, et al. 2023. Clinical validation of a wearable piezoelectric blood-pressure sensor for continuous health monitoring. *Adv. Mater.* 35:2301627
50. Yuan X, Yan A, Lai Z, Liu Z, Yu Z, et al. 2022. A poling-free PVDF nanocomposite via mechanically directional stress field for self-powered pressure sensor application. *Nano Energy* 98:107340

51. Dagdeviren C, Su Y, Joe P, Yona R, Liu Y, et al. 2014. Conformable amplified lead zirconate titanate sensors with enhanced piezoelectric response for cutaneous pressure monitoring. *Nat. Commun.* 5:4496
52. Yang Y, Pan H, Xie G, Jiang Y, Chen C, et al. 2020. Flexible piezoelectric pressure sensor based on polydopamine-modified BaTiO<sub>3</sub>/PVDF composite film for human motion monitoring. *Sens. Actuators A Phys.* 301:111789
53. Wang C, Hu Y, Liu Y, Shan Y, Qu X, et al. 2023. Tissue-adhesive piezoelectric soft sensor for in vivo blood pressure monitoring during surgical operation. *Adv. Funct. Mater.* 33:2303696
54. Sun T, Tasnim F, McIntosh RT, Amiri N, Solav D, et al. 2020. Decoding of facial strains via conformable piezoelectric interfaces. *Nat. Biomed. Eng.* 4:954–72
55. Kim Y-G, Song J-H, Hong S, Ahn S-H. 2022. Piezoelectric strain sensor with high sensitivity and high stretchability based on kirigami design cutting. *NPJ Flex. Electron.* 6:52
56. Song J-H, Kim Y-G, Cho Y, Hong S, Choi JY, et al. 2023. Stretchable strain and strain rate sensor using kirigami-cut PVDF film. *Adv. Mater. Technol.* 8:2201112
57. Dagdeviren C, Shi Y, Joe P, Ghaffari R, Balooch G, et al. 2015. Conformal piezoelectric systems for clinical and experimental characterization of soft tissue biomechanics. *Nat. Mater.* 14:728–36
58. Zhao H, Dagdeviren C, Liu G, Cao P, Wang J, et al. 2022. A new model based on the in-plane deformation for the conformal piezoelectric systems for characterization of soft tissue modulus. *Extreme Mech. Lett.* 55:101801
59. Jung YH, Hong SK, Wang HS, Han JH, Pham TX, et al. 2020. Flexible piezoelectric acoustic sensors and machine learning for speech processing. *Adv. Mater.* 32:1904020
60. Zhang Q, Wang Y, Li D, Xie J, Tao K, et al. 2023. Multifunctional and wearable patches based on flexible piezoelectric acoustics for integrated sensing, localization, and underwater communication. *Adv. Funct. Mater.* 33:2209667
61. İlik B, Koyuncuoğlu A, Şardan-Sukas Ö, Külah H. 2018. Thin film piezoelectric acoustic transducer for fully implantable cochlear implants. *Sens. Actuators A Phys.* 280:38–46
62. Persano L, Dagdeviren C, Su Y, Zhang Y, Girardo S, et al. 2013. High performance piezoelectric devices based on aligned arrays of nanofibers of poly(vinylidene fluoride-co-trifluoroethylene). *Nat. Commun.* 4:1633
63. Dagdeviren C, Joe P, Tuzman OL, Park K-I, Lee KJ, et al. 2016. Recent progress in flexible and stretchable piezoelectric devices for mechanical energy harvesting, sensing and actuation. *Extreme Mech. Lett.* 9:269–81
64. Dong K, Peng X, Wang ZL. 2020. Fiber/fabric-based piezoelectric and triboelectric nanogenerators for flexible/stretchable and wearable electronics and artificial intelligence. *Adv. Mater.* 32:1902549
65. Mahapatra SD, Mohapatra PC, Aria AI, Christie G, Mishra YK, et al. 2021. Piezoelectric materials for energy harvesting and sensing applications: roadmap for future smart materials. *Adv. Sci.* 8:2100864
66. Deng W, Zhou Y, Libanori A, Chen G, Yang W, Chen J. 2022. Piezoelectric nanogenerators for personalized healthcare. *Chem. Soc. Rev.* 51:3380–435
67. Lv P, Qian J, Yang C, Liu T, Wang Y, et al. 2022. Flexible all-inorganic Sm-doped PMN-PT film with ultrahigh piezoelectric coefficient for mechanical energy harvesting, motion sensing, and human-machine interaction. *Nano Energy* 97:107182
68. Chiu Y-Y, Lin W-Y, Wang H-Y, Huang S-B, Wu M-H. 2013. Development of a piezoelectric polyvinylidene fluoride (PVDF) polymer-based sensor patch for simultaneous heartbeat and respiration monitoring. *Sens. Actuators A Phys.* 189:328–34
69. Su Y, Chen C, Pan H, Yang Y, Chen G, et al. 2021. Muscle fibers inspired high-performance piezoelectric textiles for wearable physiological monitoring. *Adv. Funct. Mater.* 31:2010962
70. Kim D, Yang Z, Cho J, Park D, Kim DH, et al. 2023. High-performance piezoelectric yarns for artificial intelligence-enabled wearable sensing and classification. *EcoMat* 5:e12384
71. Park JJ, Won P, Ko SH. 2019. A review on hierarchical origami and kirigami structure for engineering applications. *Int. J. Precis. Eng. Manuf. Green Technol.* 6:147–61
72. Hong Y, Wang B, Lin W, Jin L, Liu S, et al. 2021. Highly anisotropic and flexible piezoceramic kirigami for preventing joint disorders. *Sci. Adv.* 7:eabf0795

73. Fu R, Zhong X, Xiao C, Lin J, Guan Y, et al. 2023. A stretchable, biocompatible, and self-powered hydrogel multichannel wireless sensor system based on piezoelectric barium titanate nanoparticles for health monitoring. *Nano Energy* 114:108617
74. Shi Y, Guan Y, Liu M, Kang X, Tian Y, et al. 2024. Tough, antifreezing, and piezoelectric organohydrogel as a flexible wearable sensor for human-machine interaction. *ACS Nano* 18:3720–32
75. Panth M, Cook B, Zhang Y, Ewing D, Tramble A, et al. 2020. High-performance strain sensors based on vertically aligned piezoelectric zinc oxide nanowire array/graphene nanohybrids. *ACS Appl. Nano Mater.* 3:6711–18
76. Dagdeviren C, Javid F, Joe P, von Erlach T, Bensele T, et al. 2017. Flexible piezoelectric devices for gastrointestinal motility sensing. *Nat. Biomed. Eng.* 1:807–17
77. Tang C, Liu Z, Hu Q, Jiang Z, Zheng M, et al. 2024. Unconstrained piezoelectric vascular electronics for wireless monitoring of hemodynamics and cardiovascular health. *Small* 20:2304752
78. Curry EJ, Ke K, Chorsi MT, Wrobel KS, Miller AN, et al. 2018. Biodegradable piezoelectric force sensor. *PNAS* 115:909–14
79. Shan Y, Wang E, Cui X, Xi Y, Ji J, et al. 2024. A biodegradable piezoelectric sensor for real-time evaluation of the motor function recovery after nerve injury. *Adv. Funct. Mater.* 34:2400295
80. Fan W, Lei R, Dou H, Wu Z, Lu L, et al. 2024. Sweat permeable and ultrahigh strength 3D PVDF piezoelectric nanoyarn fabric strain sensor. *Nat. Commun.* 15:3509
81. Ge R, Yu Q, Zhou F, Liu S, Qin Y. 2023. Dual-modal piezotronic transistor for highly sensitive vertical force sensing and lateral strain sensing. *Nat. Commun.* 14:6315
82. Dagdeviren C, Ramadi KB, Joe P, Spencer K, Schwerdt HN, et al. 2018. Miniaturized neural system for chronic, local intracerebral drug delivery. *Sci. Transl. Med.* 10:eaan2742
83. Hou JF, Nayeem MOG, Caplan KA, Ruesch EA, Caban-Murillo A, et al. 2024. An implantable piezoelectric ultrasound stimulator (ImPULS) for deep brain activation. *Nat. Commun.* 15:4601
84. Kim D, Yokota T, Suzuki T, Lee S, Woo T, et al. 2020. Ultraflexible organic light-emitting diodes for optogenetic nerve stimulation. *PNAS* 117:21138–46
85. Burton A, Wang Z, Song D, Tran S, Hanna J, et al. 2023. Fully implanted battery-free high power platform for chronic spinal and muscular functional electrical stimulation. *Nat. Commun.* 14:7887
86. Cotero V, Fan Y, Tsaava T, Kressel AM, Hancu I, et al. 2019. Noninvasive sub-organ ultrasound stimulation for targeted neuromodulation. *Nat. Commun.* 10:952
87. Lozano AM, Lipsman N, Bergman H, Brown P, Chabardes S, et al. 2019. Deep brain stimulation: current challenges and future directions. *Nat. Rev. Neurol.* 15:148–60
88. Fisher RS, Velasco AL. 2014. Electrical brain stimulation for epilepsy. *Nat. Rev. Neurol.* 10:261–70
89. Malyshev A, Goz R, LoTurco JJ, Volgushev M. 2015. Advantages and limitations of the use of optogenetic approach in studying fast-scale spike encoding. *PLOS ONE* 10:e0122286
90. Kamimura HAS, Conti A, Toschi N, Konofagou EE. 2020. Ultrasound neuromodulation: mechanisms and the potential of multimodal stimulation for neuronal function assessment. *Front. Phys.* 8:150
91. Badadhe JD, Roh H, Lee BC, Kim JH, Im M. 2022. Ultrasound stimulation for non-invasive visual prostheses. *Front. Cell. Neurosci.* 16:971148
92. Kook G, Jo Y, Oh C, Liang X, Kim J, et al. 2023. Multifocal skull-compensated transcranial focused ultrasound system for neuromodulation applications based on acoustic holography. *Microsyst. Nanoeng.* 9:45
93. Ye PP, Brown JR, Pauly KB. 2016. Frequency dependence of ultrasound neurostimulation in the mouse brain. *Ultrasound Med. Biol.* 42:1512–30
94. Seok C, Yamaner FY, Sahin M, Oralkan Ö. 2021. A wearable ultrasonic neurostimulator—part I: a 1D CMUT phased array system for chronic implantation in small animals. *IEEE Trans. Biomed. Circuits Syst.* 15:692–704
95. Thomas N, Agrawal A. 2021. Quantification of in-plane flexoelectricity in lipid bilayers. *Europhys. Lett.* 134:68003
96. Tyler WJ, Tufail Y, Finsterwald M, Tauchmann ML, Olson EJ, Majestic C. 2008. Remote excitation of neuronal circuits using low-intensity, low-frequency ultrasound. *PLOS ONE* 3:e3511
97. Kubanek J, Shi J, Marsh J, Chen D, Deng C, Cui J. 2016. Ultrasound modulates ion channel currents. *Sci. Rep.* 6:24170

98. Prieto ML, Firouzi K, Khuri-Yakub BT, Maduke M. 2018. Activation of Piezo1 but not Nav1.2 channels by ultrasound at 43 MHz. *Ultrasound Med. Biol.* 44:1217–32
99. Qiu Z, Guo J, Kala S, Zhu J, Xian Q, et al. 2019. The mechanosensitive ion channel Piezo1 significantly mediates in vitro ultrasonic stimulation of neurons. *iScience* 21:448–57
100. Hoffman BU, Baba Y, Lee SA, Tong C-K, Konofagou EE, Lumpkin EA. 2022. Focused ultrasound excites action potentials in mammalian peripheral neurons in part through the mechanically gated ion channel PIEZO2. *PNAS* 119:e2115821119
101. Kim E, Kum J, Lee SH, Kim H. 2022. Development of a wireless ultrasonic brain stimulation system for concurrent bilateral neuromodulation in freely moving rodents. *Front. Neurosci.* 16:1011699
102. Ilham SJ, Kashani Z, Kiani M. 2021. Design and optimization of ultrasound phased arrays for large-scale ultrasound neuromodulation. *IEEE Trans. Biomed. Circuits Syst.* 15:1454–66
103. Rivnay J, Wang H, Fenno L, Deisseroth K, Malliaras GG. 2017. Next-generation probes, particles, and proteins for neural interfacing. *Sci. Adv.* 3:e1601649
104. Jiang L, Lu G, Zeng Y, Sun Y, Kang H, et al. 2022. Flexible ultrasound-induced retinal stimulating piezo-arrays for biomimetic visual prostheses. *Nat. Commun.* 13:3853
105. Li S, Xu J, Li R, Wang Y, Zhang M, et al. 2022. Stretchable electronic facial masks for sonophoresis. *ACS Nano* 16:5961–74
106. Fenton OS, Olafson KN, Pillai PS, Mitchell MJ, Langer R. 2018. Advances in biomaterials for drug delivery. *Adv. Mater.* 30:1705328
107. Tan M, Xu Y, Gao Z, Yuan T, Liu Q, et al. 2022. Recent advances in intelligent wearable medical devices integrating biosensing and drug delivery. *Adv. Mater.* 34:2108491
108. Mariello M, Eş İ, Proctor CM. 2023. Soft and flexible bioelectronic micro-systems for electronically controlled drug delivery. *Adv. Healthc. Mater.* 13:2302969
109. Magisson J, Sassi A, Kobalyan A, Burcez C-T, Bouaoun R, et al. 2020. A fully implantable device for diffuse insulin delivery at extraperitoneal site for physiological treatment of type 1 diabetes. *J. Control. Release* 320:431–41
110. Nair M, Guduru R, Liang P, Hong J, Sagar V, Khizroev S. 2013. Externally controlled on-demand release of anti-HIV drug using magneto-electric nanoparticles as carriers. *Nat. Commun.* 4:1707
111. Vannozzi L, Ricotti L, Filippeschi C, Sartini S, Coviello V, et al. 2016. Nanostructured ultra-thin patches for ultrasound-modulated delivery of anti-restenotic drug. *Int. J. Nanomed.* 11:69–91
112. Sun T, Zhang YS, Pang B, Hyun DC, Yang M, Xia Y. 2014. Engineered nanoparticles for drug delivery in cancer therapy. *Angew. Chem. Int. Ed.* 53:12320–64
113. Ramadi KB, Dagdeviren C, Spencer KC, Joe P, Cotler M, et al. 2018. Focal, remote-controlled, chronic chemical modulation of brain microstructures. *PNAS* 115:7254–59
114. Vargason AM, Anselmo AC, Mitragotri S. 2021. The evolution of commercial drug delivery technologies. *Nat. Biomed. Eng.* 5:951–67
115. Nance E, Pun SH, Saigal R, Sellers DL. 2022. Drug delivery to the central nervous system. *Nat. Rev. Mater.* 7:314–31
116. Paunovska K, Loughrey D, Dahlman JE. 2022. Drug delivery systems for RNA therapeutics. *Nat. Rev. Genet.* 23:265–80
117. Mitchell MJ, Billingsley MM, Haley RM, Wechsler ME, Peppas NA, Langer R. 2021. Engineering precision nanoparticles for drug delivery. *Nat. Rev. Drug Discov.* 20:101–24
118. Azagury A, Khoury L, Enden G, Kost J. 2014. Ultrasound mediated transdermal drug delivery. *Adv. Drug Deliv. Rev.* 72:127–43
119. Prausnitz MR, Langer R. 2008. Transdermal drug delivery. *Nat. Biotechnol.* 26:1261–68
120. Boucaud A, Machel L, Arbeille B, Machel MC, Sournac M, et al. 2001. In vitro study of low-frequency ultrasound-enhanced transdermal transport of fentanyl and caffeine across human and hairless rat skin. *Int. J. Pharm.* 228:69–77
121. Pagneux Q, Ye R, Chengnan L, Barras A, Hennuyer N, et al. 2020. Electrothermal patches driving the transdermal delivery of insulin. *Nanoscale Horiz.* 5:663–70
122. Phatale V, Vaiphei KK, Jha S, Patil D, Agrawal M, Alexander A. 2022. Overcoming skin barriers through advanced transdermal drug delivery approaches. *J. Control. Release* 351:361–80

123. Park J, Lee H, Lim G-S, Kim N, Kim D, Kim Y-C. 2019. Enhanced transdermal drug delivery by sonophoresis and simultaneous application of sonophoresis and iontophoresis. *AAPS PharmSciTech* 20:96
124. Chen X, Zhu L, Li R, Pang L, Zhu S, et al. 2020. Electroporation-enhanced transdermal drug delivery: effects of logP, pK<sub>a</sub>, solubility and penetration time. *Eur. J. Pharm. Sci.* 151:105410
125. Park D, Park H, Seo J, Lee S. 2014. Sonophoresis in transdermal drug deliveries. *Ultrasonics* 54:56–65
126. Szunerits S, Boukherroub R. 2018. Heat: a highly efficient skin enhancer for transdermal drug delivery. *Front. Bioeng. Biotechnol.* 6:15
127. Karande P, Mitragotri S. 2009. Enhancement of transdermal drug delivery via synergistic action of chemicals. *Bioclim. Biophys. Acta Biomembr.* 1788:2362–73
128. He J, Zhang Y, Yu X, Xu C. 2023. Wearable patches for transdermal drug delivery. *Acta Pharm. Sin. B* 13:2298–309
129. Zeng Q, Li G, Chen W. 2023. Ultrasound-activatable and skin-associated minimally invasive microdevices for smart drug delivery and diagnosis. *Adv. Drug Deliv. Rev.* 203:115133
130. Polat BE, Hart D, Langer R, Blankschtein D. 2011. Ultrasound-mediated transdermal drug delivery: mechanisms, scope, and emerging trends. *J. Control. Release* 152:330–48
131. Tuan-Mahmood T-M, McCrudden MTC, Torrisi BM, McAlister E, Garland MJ, et al. 2013. Microneedles for intradermal and transdermal drug delivery. *Eur. J. Pharm. Sci.* 50:623–37
132. Prausnitz MR. 2004. Microneedles for transdermal drug delivery. *Adv. Drug Deliv. Rev.* 56:581–87
133. Yang Y, Xu L, Jiang D, Chen BZ, Luo R, et al. 2021. Self-powered controllable transdermal drug delivery system. *Adv. Funct. Mater.* 31:2104092
134. Wu Q, Pan C, Shi P, Zou L, Huang S, et al. 2023. On-demand transdermal drug delivery platform based on wearable acoustic microneedle array. *Chem. Eng. J.* 477:147124
135. Zhao Z, Saiding Q, Cai Z, Cai M, Cui W. 2023. Ultrasound technology and biomaterials for precise drug therapy. *Mater. Today* 63:210–38
136. Kossoff G. 2000. Basic physics and imaging characteristics of ultrasound. *World J. Surg.* 24:134–42
137. Nyborg WL. 2002. Safety of medical diagnostic ultrasound. *Semin. Ultrasound CT MRI* 23:377–86
138. Zhou Q, Lam KH, Zheng H, Qiu W, Shung KK. 2014. Piezoelectric single crystal ultrasonic transducers for biomedical applications. *Prog. Mater. Sci.* 66:87–111
139. Yin J, Tao C, Liu X. 2017. Dynamic focusing of acoustic wave utilizing a randomly scattering lens and a single fixed transducer. *J. Appl. Phys.* 121:174901
140. dos Santos MJSF, dos Santos JB. 2011. FPGA-based control system of an ultrasonic phased array. *Strog. vestn. J. Mech. Eng.* 57(2):135–41
141. Bhuyan A, Choe JW, Lee BC, Cristman P, Oralkan Ö, Khuri-Yakub BT. 2011. Miniaturized, wearable, ultrasound probe for on-demand ultrasound screening. In *Proc. 2011 IEEE International Ultrasonics Symposium, Orlando, FL, USA, October 18–21, 2011*, pp. 1060–63. New York: IEEE
142. Harput S, Christensen-Jeffries K, Ramalli A, Brown J, Zhu J, et al. 2020. 3-D super-resolution ultrasound imaging with a 2-D sparse array. *IEEE Trans. Ultrason. Ferroelectr. Freq. Control* 67:269–77
143. Feigenbaum H. 2010. Role of M-mode technique in today's echocardiography. *J. Am. Soc. Echocardiogr.* 23:240–57
144. Kenny J-ÉS, Munding CE, Eibl JK, Eibl AM, Long BF, et al. 2021. A novel, hands-free ultrasound patch for continuous monitoring of quantitative Doppler in the carotid artery. *Sci. Rep.* 11:7780
145. Lin M, Zhang Z, Gao X, Bian Y, Wu RS, et al. 2024. A fully integrated wearable ultrasound system to monitor deep tissues in moving subjects. *Nat. Biotechnol.* 42:448–57
146. Zhang L, Marcus C, Lin D, Mejorado D, Schoen SJ, et al. 2024. A conformable phased-array ultrasound patch for bladder volume monitoring. *Nat. Electron.* 7:77–90
147. Liu H-C, Zeng Y, Gong C, Chen X, Kijanka P, et al. 2024. Wearable bioadhesive ultrasound shear wave elastography. *Sci. Adv.* 10:eadk8426
148. Wang C, Chen X, Wang L, Makihata M, Liu H-C, et al. 2022. Bioadhesive ultrasound for long-term continuous imaging of diverse organs. *Science* 377:517–23
149. Taljanovic MS, Gimber LH, Becker GW, Latt LD, Klauser AS, et al. 2017. Shear-wave elastography: basic physics and musculoskeletal applications. *RadioGraphics* 37:855–70

150. China D, Feng Z, Hooshangnejad H, Sforza D, Vagdargi P, et al. 2024. FLEX: flexible transducer with external tracking for ultrasound imaging with patient-specific geometry estimation. *IEEE. Trans. Biomed. Eng.* 71:1298–307
151. Huang X, Bell MAL, Ding K. 2021. Deep learning for ultrasound beamforming in flexible array transducer. *IEEE Trans. Med. Imaging* 40:3178–89
152. Bosco E, Spairani E, Toffali E, Meacci V, Ramalli A, Matrone G. 2024. A deep learning approach for beamforming and contrast enhancement of ultrasound images in monostatic synthetic aperture imaging: a proof-of-concept. *IEEE Open J. Eng. Med. Biol.* 5:376–82
153. Beard P. 2011. Biomedical photoacoustic imaging. *Interface Focus* 1:602–31
154. Lin L, Wang LV. 2022. The emerging role of photoacoustic imaging in clinical oncology. *Nat. Rev. Clin. Oncol.* 19:365–84
155. Gao X, Chen X, Hu H, Wang X, Yue W, et al. 2022. A photoacoustic patch for three-dimensional imaging of hemoglobin and core temperature. *Nat. Commun.* 13:7757
156. Griffin MF, Leung BC, Premakumar Y, Szarko M, Butler PE. 2017. Comparison of the mechanical properties of different skin sites for auricular and nasal reconstruction. *J. Otolaryngol. Head Neck Surg.* 46:33
157. Sirohi J, Chopra I. 2000. Fundamental understanding of piezoelectric strain sensors. *J. Intell. Mater. Syst. Struct.* 11:246–57